SKI Report 02:39

Research

Buffering Capacity of pH in Backfill

Steven Benbow
Peter Robinson
David Savage

August 2002

ISSN 1104–1374
ISRN SKI-R-02/39-SE

SKI perspective

Background

Concrete and cement are used in constructions as well as in conditioning of waste in repositories for radioactive waste. In an earlier review of SKB's preliminary safety assessment of the repository for long-lived low- and intermediate-level waste (SFL 3-5) SKI has questioned the SKB results regarding neutralisation of high pH in backfill. According to SKB, the cementitious pore water leached from the concrete would be neutralised by only a small amount of the quartz in the backfill.

If it can not be excluded that groundwater in the backfill and bedrock adjacent to the backfill becomes highly alkaline, all potential consequences (change of water chemistry, influence on sorption and solubilities etc.) must be evaluated in the performance assessment context.

Purpose of the project

The aim of the current project has been to review recent work published by SKB on potential reaction mechanisms and assessments of the potential pH buffering capacity of gravel backfills. Scoping calculations have been carried out on a particle scale to investigate uncertainties encountered by different dissolution models, mineral compositions and diffusional transport.

Results

The approaches used by SKB to model the potential for buffering of hydroxyl ions released by cementitious engineered barriers are considered to have a number of deficiencies. In particular, non-conservative estimates are used for the amount of hydroxyl ions which may be consumed by precipitation of CSH (calcium silicate hydrates) minerals, as well as for the amount of quartz in the backfill. Further, SKB's choice of rate-limiting step in the process is not consistent with experimental results.

In this study different models has been tested for the dissolution of quartz, and revealed that the interior of the particle becomes shielded from the cement water by a layer of CSH precipitates. The possible amount of buffering is thus much smaller than claimed by SKB.

Continued work

The work is planned to be continued by modelling on repository scale. It will aim to investigate if and how the difference in hydraulic conductivity between the repository structures and the filling material would influence the pH buffering capabilities.

Effects on SKI work

The current report results will be applicable also for other repositories, cementitious based like e.g. the low-level waste repository (SFR 1) in Forsmark, as well as for the

planned spent fuel repository (if significant amounts of cementitious materials are used). The result will also be used to assist SKI in its review of SKB's renewed safety assessment for SFR 1.

Project information

Responsible for the project at SKI has been Christina Lilja.
SKI reference: 14.9-011255/01265.

Other relevant SKI Reports:
Joint SKI and SSI review of SKB preliminary safety assessment of repository for long-lived and intermediate-level waste, Review report, SKI Report 01:34, Swedish Nuclear Power Inspectorate, 2001.

SKI Report 02:39

Research

Buffering Capacity of pH in Backfill

Steven Benbow[1]
Peter Robinson[1]
David Savage[2]

[1]Quintessa Ltd., Dalton House, Newton Road
Henley-on-Thames, Oxfordshire RG9 1HG
United Kingdom

[2]Quintessa Ltd., 24 Trevor Road
West Bridgford, Nottingham NG2 6FS
United Kingdom

August 2002

SKI Project Number 01265

Contents

			Page
1	**Introduction**		**1**
2	**Discussion of ”Possible buffering of pH-plume by silicate in the sand/gravel buffer” (SKB Report R-99-15, Appendix B)**		**2**
	2.1	Mass balance	2
	2.2	Reaction depth in sand/gravel particles	5
	2.3	Diffusion of OH^- from concrete	7
	2.4	Summary	9
3	**Modelling**		**10**
	3.1	The Raiden2 geochemical model	10
	3.2	Particle-scale modelling	15
		3.2.1 Model input considerations	17
		3.2.2 Results	27
		3.2.3 Summary	45
4	**Conclusions**		**46**
5	**References**		**48**

Summary

Gravel backfills may help retard the migration of hyperalkaline cement pore fluids in repository designs containing large amounts of cement and concrete (e.g. the proposed Swedish SFL 3-5 repository) by acting as a 'sacrificial' reactive barrier. This behaviour relies on the reaction of silicate and aluminosilicate minerals in the backfill through hydroxyl ion-catalysed mineral dissolution reactions and the associated precipitation of hydroxyl ion bearing solids, such as calcium silicate hydrates. Recent work published by SKB on potential reaction mechanisms and assessment of the potential performance of such backfills has been reviewed, and scoping calculations to assess likely backfill performance have been carried out.

The approaches and methodologies employed by SKB to model the potential for buffering of hydroxyl ions released by cementitious engineered barriers by reaction with a surrounding gravel barrier are considered to have a number of deficiencies. In particular, mass balance calculations used a non-conservative estimate of the amount of hydroxyl ions which may be consumed by precipitation of CSH minerals. More conservative choices of the composition of CSH suggest that complete reaction of at least 36 % of the gravel barrier (as currently designed), and possibly much more, would be required to contain the release of all hydroxyl ions contained within cement in SFL 3-5. Also, SKB's scoping calculations overestimate the amount of quartz/SiO_2 likely to be present in the gravel backfill, thus leading to an overestimation of the likely amount of retardation of hydroxyl ion migration through the backfill. Moreover, SKB's calculations assumed that the reactive surface area of particles in the gravel backfill does not change with time and that the rate-limiting step of release of silica remains detachment of silicate ions from the mineral surfaces. However, evidence from SKB's own experiments suggests that the surface area available for dissolution will decrease with time due to the coating of surfaces by precipitates and it is likely that the rate-limiting step for release of Si (and hence OH^- consumption) ultimately becomes diffusion through an alteration layer of precipitates surrounding rock fragments.

Modelling of quartz-water reactions at the particle-scale carried out in this study using different plausible models for the dissolution of quartz has revealed that the total amount of buffering of the cement water provided by diffusion into, and reaction in, the particle pore space is small and is not enough to satisfy the amounts of buffering claimed by SKB. In every model case, the interior of the particle becomes shielded from the cement water by a layer of CSH that precipitates in the pore space adjacent to the surface, thus removing the interior of the particle from further reaction.

1 Introduction

Gravel backfills may help retard the migration of hyperalkaline cement pore fluids in repository designs for radioactive waste containing large amounts of cement and concrete (e.g. the proposed Swedish SFL 3-5 repository) by acting as a 'sacrificial' reactive barrier. This behaviour relies on the reaction of silicate and aluminosilicate minerals in the backfill through hydroxyl ion-catalysed mineral dissolution reactions and the associated precipitation of hydroxyl ion bearing solids, such as calcium silicate hydrates.

Recent work published by SKB (Karlsson et al., 1999) on potential reaction mechanisms and an assessment of the potential performance of such backfills has suggested that OH^- ions in the migrating cement pore fluids may be wholly consumed by dissolution of quartz in gravel backfills of broad 'granitic' composition and subsequent precipitation of calcium silicate hydrate (CSH) solids. One of the conclusions of this work was that only a small portion of the total amount of quartz in the backfill (< 6 %) was needed to buffer pH in the regime pH 7-8 over relatively short timescales (a few years). Consequently, Karlsson et al. (1999) concluded that:

> *"… it is possible to assume that the occurrence of a plume of hydroxide ions with a relatively high pH is limited to the sand/gravel backfill and the influence of the plume on the rock mass is considered to be insignificant"*.

In March 2001, SKI concluded its review of SKB's preliminary safety assessment of the SFL 3-5 repository (SKI, 2001). In this review, the validity of the concept of complete neutralisation of hyperalkaline pore fluids migrating from the cementitious barriers by reaction with a gravel backfill proposed by SKB was questioned by an international panel of experts helping SKI with its review.

The aim of the work presented here is to review the work conducted by SKB regarding chemical buffering by a gravel backfill and to conduct model calculations to investigate the validity of SKB's claims for the performance of this proposed engineered barrier design for SFL 3-5.

2 Discussion of ”Possible buffering of pH-plume by silicate in the sand/gravel buffer” (SKB Report R-99-15, Appendix B)

The SKB report by Karlsson et al. (Karlsson et al., 1999) describes potential mechanisms and mass balances concerning the retardation of a ‘plume’ of hyperalkaline pore fluid emanating from cement and concrete in the engineered barrier system of a Swedish deep repository for long-lived low- and intermediate level radioactive wastes. Although aimed principally at the repository designated ‘SFL 3-5’, much of Karlsson et al.’s discussion could also be applicable to other repository types involving both cement/concrete and sand, gravel, or bentonite backfills.

Karlsson et al. (1999) present their arguments in terms of 3 approaches, namely:

- Mass balance;
- Reaction depth in sand/gravel particles;
- Diffusion of OH^- from concrete and dissolution of SiO_2.

This layout will be followed here.

2.1 Mass balance

Initially, Karlsson et al. (1999) consider the mass balance of OH^- present in cement and concrete and the total amount of SiO_2 in the gravel backfill which is theoretically available for neutralisation of the hydroxyl ions by chemical reaction.

The total amount of concrete in the various parts of SFL 3-5 arrived at in this manner is 32 207 m^3, with the total amount of sand/gravel backfill being 70 069 m^3. Using typical chemical compositional data for concrete and granite, Karlsson et al. calculate total amounts (moles) of OH^- in concrete and SiO_2 in granite to be 4.86×10^7 and 6.62×10^8, respectively.

Karlsson et al. go on to state that the most likely product of the interaction between hydroxyl and silicate ions is solid calcium silicate hydrate (CSH). This assumption is well founded, since many authors have noted the reactivity of calcium ions at elevated pH in the presence of aqueous silica species (e.g. Henning and Gerstner, 1972; Kondo, 1967). CSH solids will form even during the period of cement pore fluids dominated by Na-K hydroxides (e.g. Savage et al., 1992). Karlsson et al. (Karlsson et al., 1999) do not specify a stoichiometry for the CSH phase which they expect to precipitate, but consider that the ratio of hydroxyl ions to aqueous silica species in this phase would be two. Using this ratio and their calculated amounts of hydroxyl and silicate ions in concrete and backfill respectively, Karlsson et al. thus conclude that only 7 % of the available silica would be needed to effect precipitation of the entire content of hydroxyl ions in the concrete in SFL 3-5.

The amounts of hydroxyl and silicate ions calculated by Karlsson et al. to be present in the engineered barrier system of SFL 3-5 are taken here to be an accurate estimate. However, the conservatism of the assumption made by Karlsson et al. regarding the OH/Si ratio of the product CSH phase is discussed in more detail below.

A reaction for the precipitation of CSH of general formula $Ca_xSi_yO_{(x+2y)}.wH_2O$ is as follows:

$$x\mathrm{Ca}^{2+} + y\mathrm{H_3SiO_4^-} + (2x\text{-}y)\mathrm{OH^-} = \mathrm{Ca_xSi_yO_{(x+2y)}}w\mathrm{H_2O} + (x+y\text{-}w)\mathrm{H_2O} \quad (1)$$

Whether such reactions neutralise hyperalkaline fluids, i.e. consume OH^- (or generate H^+), depends upon the precise stoichiometry of the CSH solid concerned, and in particular the magnitude of the '2*x*-*y*' parameter (above). *Table 1* presents compositional data for some naturally-occurring CSH minerals, together with information regarding Ca/Si (solid) and $OH^-/H_3SiO_4^-$ (fluid) ratios, and the '2*x*-*y*' parameter defined above.

Table 1 Some naturally-occurring calcium silicate hydrate minerals.

Mineral	**Formula**	**Ca/Si ratio**	**$OH^-/H_3SiO_4^-$**	**'2*x*-*y*'**
Hillebrandite	Ca_2SiO_4:1.17H_2O	2.00	3.00	3
Afwillite	$Ca_3Si_2O_4(OH)_6$	1.50	2.00	4
Foshagite	$Ca_4Si_3O_{10}$:1.5H_2O	1.33	1.66	5
Xonotlite	$Ca_6Si_6O_{18}$:H_2O	1.00	1.00	6
Tobermorite	$Ca_5Si_6O_{17}$:10.5H_2O	0.83	0.66	4
Gyrolite	$Ca_2Si_3O_8$:2.5H_2O	0.67	0.33	1
Okenite	$CaSi_2O_5$:2H_2O	0.50	0	0

It may be seen from *Table 1* that CSH minerals cover a range of both Ca/Si (from 0.5 to 2) and $OH^-/H_3SiO_4^-$ (from 0 to 3) ratios, so that there is a range of capacity to 'neutralise' hydroxyl ions. For example, the precipitation of one mole of the CSH mineral xonotlite, $Ca_6Si_6O_{18}.H_2O$ (2*x*-*y* = 6) consumes six moles of hydroxyl ions:

$$6Ca^{2+} + 6H_3SiO_4^- + 6OH^- = Ca_6Si_6O_{18}.H_2O + 11H_2O \qquad (2)$$

whereas the precipitation of the mineral okenite, $CaSi_2O_5$:2H_2O (2*x*-*y* = 0) does not consume any hydroxyl ions:

$$Ca^{2+} + 2H_3SiO_4^- = CaSi_2O_5.2H_2O + H_2O \qquad (3)$$

The choice of which CSH phase to include in a mass balance thus becomes crucial. Typically, the Ca/Si ratio of the CSH precipitate depends upon the ratio in the fluid, and in a closed system, this ratio decreases with time as Ca is progressively removed from the fluid (Savage et al., 1992). It can be seen from *Table 1* that the CSH solid chosen by Karlsson et al. for their mass balance calculation corresponds to afwillite (Ca/Si = 1.5; $OH^-/H_3SiO_4^-$ = 2). It should be noted that this solid has the second largest $OH^-/H_3SiO_4^-$ ratio of all the CSH minerals presented in *Table 1* and is thus relatively beneficial with regard to its ability to incorporate OH^- ions.

It is debatable which composition of CSH solid would most likely form in the envisaged disposal environment for SFL 3-5, but the composition chosen by Karlsson et al. is not especially conservative (i.e. pessimistic with respect to OH^- retardation). In a laboratory experimental study of the alteration of typical 'granitic' minerals (quartz, feldspars, micas) by hyperalkaline Na-K-Ca-OH fluids, Savage et al. (1992) noted that Ca/Si ratios of CSH products ranged from 0.5 to 1.5, i.e. from 'okenite' to 'afwillite' in composition. Bateman et al. (1999) noted a similar range of composition for CSH products from the reaction of columns of minerals such as quartz, feldspars and micas with hyperalkaline fluids.

Consequently, if a CSH solid with a Ca/Si ratio towards the lower end of this range is chosen (i.e. 'gyrolite', Ca/Si = 0.67; $OH^-/H_3SiO_4^-$ = 0.33) for $OH^-/H_3SiO_4^-$ mass balance calculations at SFL 3-5, then approximately six times the amount of silica in the granite backfill calculated by Karlsson et al. (1999) would be needed for reaction, i.e. 36 % of the total backfill inventory. Although this figure is still within the total inventory of silicate backfill currently planned for SFL 3-5, it demonstrates that a considerably larger fraction of the backfill could be required for reaction than that envisaged by Karlsson et al. If the chemical composition of the CSH solid approaches that with the lowest observed in laboratory experimental studies (i.e. 'okenite', Ca/Si =0.5; $OH^-/H_3SiO_4^-$ = 0), then an infinite amount of gravel backfill would be required to retard the migration of OH^- ions from the cement and concrete portion of the EBS.

2.2 Reaction depth in sand/gravel particles

Karlsson et al. (1999) recognised that arguments relating to a simple mass balance of hydroxyl and silicate ions were insufficient to guarantee retardation of hyperalkaline pore fluids within the SFL 3-5 engineered barrier system. Since dissolution of silicate and aluminosilicate minerals is a surface-dependent process (e.g. Brady and Walther, 1989), reactive surface areas and particle reaction depths must also be considered.

Karlsson et al. correctly state that the reaction depth, *s*, for a spherical particle of radius

r needed to produce a given fraction *X* reacted is given by:

$$s = r - \left(r^3 - r^3 X\right)^{1/3} \tag{4}$$

For small *X*, as is relevant here, this expression can be approximated by:

$$s = r\frac{X}{3} = X\frac{V}{A} \tag{5}$$

This implies that for a particle diameter of 10 mm (radius 5 mm) say, and a reacted fraction of 6 %, then a reacted depth should be of the order of 0.1 mm. The Figures produced by Karlsson et al. (1999) accurately reflect this.

Karlsson et al. (1999) go on to discuss average particle size of the backfill and produce the following expression to describe the average particle size of backfill with particles in the range 4 – 32 mm in diameter:

$$d_{av} = \left(\frac{\left(d_{\min}^3 + d_{\max}^3\right)}{2}\right)^{1/3} = \left(\frac{\left(4^3 + 32^3\right)}{2}\right)^{1/3} = 25\ \text{mm} \tag{6}$$

Unfortunately, this expression is not strictly appropriate since (6) assumes that half the particles are 4 mm in diameter and the other half are 32 mm in diameter. In reality, the average particle size can only be evaluated from a particle size distribution. However, the average volume will probably be dominated by the largest particles, so that 25 mm as an estimate of the average particle size may be a reasonable estimate.

Karlsson et al. (1999) then discuss the results of laboratory experiments reacting rock pieces in concrete porewater at 70 °C for six months (Holgersson et al., 1998) as a means of determining the likely alteration depth of rock particles in backfill and also as potential corroboration of their calculations. The size of the particulates used in the experiments is not stated by Karlsson et al. (1999), but they suggest that the depth of alteration observed experimentally (of the order of 50 μm) is much less than expected. Karlsson et al. (1999) explain this discrepancy by a likely difference between the

'geometric' surface area in their model and the area of rough particles in the experiments. Although it is likely that geometric area will underestimate the surface area of rough particles and thus contribute towards the discrepancy between modelled and experimental evidence, contributory factors ignored by Karlsson et al. (1999) are the likely effects of 'armouring' of the rock particles by precipitates (thus adding a transport effect upon the release of silica by rock dissolution), and that of reaction kinetics of silicate mineral dissolution. Both these effects will contribute to a decreased amount of alteration than that predicted by Karlsson et al.'s model.

2.3 Diffusion of OH^- from concrete and dissolution of SiO_2

The final approach taken by Karlsson et al. (1999) is to evaluate the balance between diffusion of OH^- ions from concrete and their removal from solution by reaction with dissolving silicate minerals in the backfill. A simple explicit time-stepping algorithm is used to estimate the amount of OH^- ions released by diffusion and those consumed by dissolution of quartz. The concrete is treated as a semi-infinite plate and the gravel backfill has no spatial discretisation. A backfill particle size of 25 mm was chosen for the calculations.

Laboratory experimental data for surface area- and pH-dependent quartz dissolution from Knauss and Wolery (1988) were employed as the rate-limiting step in OH^- consumption. Although it is not stated explicitly by Karlsson et al. (1999), it is assumed here that they may have envisaged the following relationship for consumption of hydroxyl ions by quartz dissolution:

$$SiO_2 + OH^- + H_2O = H_3SiO_4^- \qquad (7)$$

In this case, one hydroxyl ion is consumed for every mole of quartz dissolved.

A factor which should not be ignored in this respect is that the experimental data utilised in the calculations refer to quartz dissolution, i.e. a phase consisting of 100 % SiO_2, whereas the rock back fill envisaged for SFL 3-5 would consist of only 30 %

quartz, or 60-65 % total SiO_2. This does not seem to have been incorporated into the calculations reported by Karlsson et al. (1999), so that their results will overestimate the amount of silica released (by a factor of approximately 1.5 to 3) and hence, overestimate the amount of OH^- consumed.

Notwithstanding these uncertainties, Karlsson et al. (1999) calculate that the diffusion of OH^- from the concrete is slower than the release of SiO_2 from quartz dissolution and thus the pH of the pore fluid in the gravel backfill decreases to below pH 9 after only a few years (< 5 years) for all portions of the SFL 3-5 repository.

Karlsson et al. (1999) also discuss the time to achieve depletion of portlandite in the concrete in SFL 3-5, and draw analogy with previous calculations carried out by Höglund and Bengtsson (1991) for the SFR repository together with archaeological analogue studies of concrete water tanks. However, since hydroxyl ions will be released from concrete by calcium silicate hydrate gel dissolution long after portlandite has been removed, it is not entirely clear why these calculations are included by Karlsson et al. (1999).

Again, the principal deficiency in the calculations presented by Karlsson et al. (1999) is the assumption that the reactive surface area of the quartz/rock fragments in the gravel backfill remains constant with time and that the rate-limiting step is detachment of silicate ions from the structures of the silicate minerals. As SKB's own laboratory experiments on this topic (e.g. Holgersson et al., 1998; Bateman et al., 1999) indicate however, considerable thicknesses (10's of microns) of precipitates (principally CSH solids) will coat the reactive silicates in relatively short time periods of weeks/months. Consequently, it is more likely that the rate-limiting step regarding release of silica will become diffusion through a layer of alteration products. Therefore it is the processes of decreasing effective surface area with time and transport through alteration layers which need to be incorporated into a model of pH buffering in backfill.

2.4 Summary

The approaches and methodologies employed by Karlsson et al. (1999) to model the potential for buffering of hydroxyl ions released by cementitious engineered barriers by reaction with a surrounding gravel barrier have been reviewed and are considered to have a number of deficiencies, namely:

- Mass balance calculations have used a non-conservative estimate of the amount of hydroxyl ions which may be consumed by precipitation of CSH minerals. More conservative choices of the composition of CSH suggest that complete reaction of at least 36 % of the gravel barrier (as currently designed), and possibly much more, would be required to contain the release of all hydroxyl ions contained within SFL 3-5.
- Formulae to calculate the average particle diameter in the gravel backfill are inappropriate for the likely nature of the material concerned. Although these formulae may not introduce large errors in subsequent calculations, they are incorrect and should be revised.
- Calculations involving quartz dissolution assume that backfill particles consist of 100 % SiO_2 and thus overestimate the amount of quartz/SiO_2 likely to be present in the gravel backfill, thus leading to an overestimation of the likely amount of retardation of hydroxyl ion migration through the backfill.
- All calculations have assumed that the reactive surface area of particles in the gravel backfill does not change with time and that the rate-limiting step of release of silica remains detachment of silicate ions from the mineral surfaces. Evidence from SKB's own experiments suggests that the surface area available for dissolution will decrease with time due to the coating of surfaces by precipitates and it is likely that the rate-limiting step for release of Si (and hence OH^- consumption) ultimately becomes diffusion through an alteration layer surrounding rock fragments.

3 Modelling

The potential for the retardation of hyperalkaline pore fluids from cement by chemical reaction in a gravel backfill has been modelled using the modelling tool *Raiden2*. *Raiden2* is a 2-D reactive geochemistry and fully coupled transport code developed by Quintessa that allows a variety of reaction mechanisms to be modelled in 2-D heterogeneous media. Such a model allows an analysis of the changing mineralogy and pore water chemistry in the backfill as a function of time to be made.

In the following sections, a description of the fundamental equations in the *Raiden2* code is presented, followed by descriptions of particle-scale modelling with results being compared to those stated in Karlsson et al. (1999).

3.1 The *Raiden2* geochemical model

Particle-scale pH buffering issues have been investigated using *Raiden2*, which is a software tool for solving fully coupled geochemical transport problems in two spatial dimensions. This section describes the fundamental equations governing the geochemical evolution that are solved by *Raiden2*.

The user sets up a *Raiden2* problem by defining the initial (possibly heterogeneous) mineralogical and pore water chemical conditions in the system and some pore water boundary conditions on the system. These, together with further parameters that define the host medium (porosity, hydraulic conductivity, storativity, etc.), transport coefficients (diffusion coefficients, dispersion coefficients, etc.), groundwater boundary conditions (groundwater composition and hydraulic head) and reaction equations that are assumed for each mineral species are sufficient to prescribe a set of equations that can be solved for the evolution of the system. *Raiden2* uses a non-uniform, user-defined discretisation of the domain into cells. One or two-dimensional grids are supported in either Cartesian or cylindrical-polar coordinates.

In the *Raiden2* model, chemical species in the system are characterised as either

- mineral species,
- aqueous complex species, or
- basis species.

Mineral species are assumed to be stationary, and hence not susceptible to transport through the pore space, aqueous complex species are those aqueous species that are composed of a combination of the basis species, which are the fundamental building blocks of the chemical system. All of the mineral and aqueous complex species must be expressible as a combination of the basis species. The medium itself is assumed to be composed of the mineral species, with all other solid in the medium being composed of an inert solid that is not involved in any geochemical reactions.

The i^{th} mineral species is denoted by M_i (mol/m^3), i^{th} aqueous complex species is denoted by c_i (mol/l) and the i^{th} basis species is denoted by b_i (mol/l). Then, the total aqueous concentration of basis species i, b_i^{aq} (mol/l), and the total concentration per unit volume of basis species i, b_i^{tot} (mol/m^3) are given by:

$$b_i^{aq} = b_i + \sum_{j=1}^{N_c} \nu_{ij} c_j \tag{8}$$

$$b_i^{tot} = S\phi b_i^{aq} + \sum_{j=1}^{N_M} \gamma_{ij} m_j \tag{9}$$

where N_C is the number of aqueous complex species, N_M is the number of mineral species, ν_{ij} is the stoichiometry of basis i in aqueous complex j, γ_{ij} is the stoichiometry of basis i in mineral j, ϕ is the porosity and S is a volumetric scale factor. The number of basis species is denoted N_B.

The transport equation for the i^{th} basis species is then

$$\frac{\partial}{\partial t}\left[S\phi b_i^{aq} + \sum_{j=1}^{N_M} \gamma_{ij} m_j \right] = S\left\{ \nabla \cdot \left[\phi D_{B_i} \nabla b_i + \sum_{j=1}^{N_c} \phi D_{C_j} \nabla c_j \right] - \nabla \cdot \left[q b_i^{aq} \right] \right\} \tag{10}$$

Here, D_{Z_i} is the total dispersion coefficient of the i^{th} (either basis or aqueous complex) species,

$$\phi D_{Z_i} = \alpha_{Z_i} q + \phi D_{Z_i}^{mol} \tag{11}$$

where α_{Z_i} is the longitudinal dispersion coefficient (m) for the i^{th} (either basis or aqueous complex) species, q is the Darcy velocity (m/s) and $D_{Z_i}^{mol}$ is the molecular diffusion coefficient for the i^{th} (either basis or aqueous complex) species.

The rate of dissolution/precipitation of the i^{th} mineral species can be set either as an explicit kinetic rate equation, or as an implicit rate equation where instantaneous dissolution/precipitation of the mineral is assumed in order for the mineral to be instantaneously in equilibrium with the pore water. For kinetic dissolution and precipitation reactions, the user must choose a representative kinetic reaction for each mineral from *Raiden2*'s (extensible) reaction library, and parameterise it appropriately. The general form of the explicit kinetic equations is:

$$\frac{dm_i}{dt} = F\left(\{b_j : j = 1,\ldots,N_B\}, \{c_j : j = 1,\ldots,N_c\}, \{m_j : j = 1,\ldots,N_M\}, K_{M_i}(T), I, T \right) \tag{12}$$

where K_{M_i} is the temperature dependent equilibrium constant for the i^{th} mineral species, I is the ionic strength of the pore water, T is the temperature and $F(\cdot)$ denotes a function of the parameters, i.e. the kinetic reaction rate can be any function of the pore water chemistry, mineralogy, ionic strength and temperature in each cell in the discretisation. It is unlikely that many mineral reactions will be characterised in terms of concentrations of other minerals or complex species, instead it will usually be the case that mineral reaction rates are a function of their surface area (and hence of their concentration, specific surface area and molar volume), their equilibrium state (and hence of those basis species with non-zero stoichiometry in the mineral), and also of

one or two specific basis species, most commonly H^+. However, the ability to characterise reactions in terms of other mineral concentrations and aqueous complex concentrations has been included in *Raiden2* for maximum flexibility, and can be important if considering solid solution reactions. The implicit instantaneous equilibrium equations are set up automatically in *Raiden2* (if the user chooses that this should be done).

The aqueous complex species are assumed to be in instantaneous equilibrium with the pore water at all times, so that

$$Q_{C_i} = K_{C_i}(T) \tag{13}$$

at all times, where K_{C_i} is the temperature dependent equilibrium constant for the i^{th} aqueous complex species, and Q_{C_i} is the equilibrium state of the i^{th} aqueous complex species, i.e.

$$Q_{C_i} = \prod_{j=1}^{N_B} \left[\mu_j(I) b_j\right]^{\gamma_{ij}} \tag{14}$$

where μ_j is the activity coefficient of the j^{th} basis species.

Porosity change in the medium is given by:

$$\frac{d\phi}{dt} = -\sum_{i=1}^{N_M} V_i^{mol} \frac{dm_i}{dt} \tag{15}$$

where V_i^{mol} is the molar volume of the i^{th} mineral.

Flow in the region is fully coupled with porosity change and varies according to

$$S_s \frac{\partial h(x)}{\partial t} = \nabla \cdot [K(x) \nabla h] - \frac{\partial \phi}{\partial t} + Q \tag{16}$$

Here Q is the volume flow rate of pore water per unit volume (s^{-1}) and S_s is the storativity coefficient (m^{-1}), which is given by:

$$S_s = \rho_{aq} g \left[\zeta_{aq} \phi + \sum_{i=1}^{N_M} \zeta_{M_i} V_i m_i + \zeta_I (1 - \phi_I) \right] \tag{17}$$

where ρ_{aq} is the fluid density, g is gravitational acceleration, ζ_I is the compressibility of any inert components of the medium, ζ_{aq} is the compressibility of the fluid, ζ_{M_i} is the compressibility of the i^{th} mineral species and ϕ_I is the portion of the volume (of everything) that is filled with inert materials.

Raiden2 makes use of two databases, the reaction library (which was introduced in the previous section) and also the EQ3/6 database (Wolery, 1992). *Raiden2* uses the EQ3/6 database to determine:

- Relevant basis species for each mineral in the model.
- Relevant basis species for each aqueous complex in the model.
- Stoichiometries of the basis species in each mineral and complex species.
- Temperature-dependent equilibrium constants for each aqueous complex and mineral species.
- Molar volumes and molar weights for each mineral, aqueous complex and basis species.

3.2 Particle-scale modelling

Karlsson et al. (1999) cite an experimental result from Holgersson et al. (1998), where a study was made of the evolution of rock pieces that were stored in cementitious water for 6 months. The results of Holgersson et al. (1998) are summarised in Karlsson et al. (1999) as follows:

> *"Rock pieces, which were stored in concrete pore water at 70 °C for 6 months were observed to have a penetration depth of less than 50 μm."*

Having calculated the total amount of OH^- that could possibly be leached from the concrete, Karlsson et al. (1999) then calculated the total amount of SiO_2 that would be needed to buffer the total OH^- in the pore fluid. The amount of SiO_2 that was needed was written as X % of the total amount of SiO_2 in the backfill. The values of X % that were calculated were found to be mostly around 4 %, with the exception of a 1 % value for SFL-4. These percentages were derived using the assumption that one mole of SiO_2 in the backfill reacts with (removes) two moles of OH^- from the pore fluid. This assumption was discussed at length in Section 2 above (where it was noted that Karlsson et al. had implicitly assumed a CSH phase of afwillite composition) and was found to be non-conservative to the extent that choosing minerals with Ca/Si ratios nearer 0.5 to represent the CSH phase would result in six times as much SiO_2 being required to buffer the pH plume as Karlsson et al. (1999) predicted.

Assuming spherical granite particles and assuming that all particles are equally altered by the pH plume (regardless of their spatial location), Karlsson et al. (1999) were then able to characterise the "*penetration depth*", s, within the particles as a function of the initial radius of the particle, r, and X (see *Figure 1a*):

$$s = r - (r^3 - r^3X)^{1/3} \qquad (18)$$

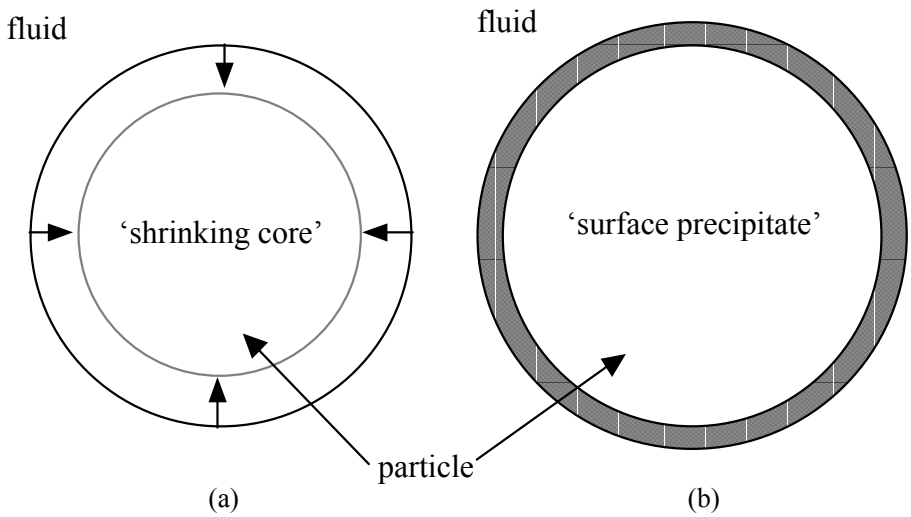

Figure 1 Schematic illustration of the two conceptual models of reaction. (a) is a 'shrinking core' model where an alteration zone moves into the particle. (b) is a model where alteration products accumulate on the surface of the particle and particle reaction is a surface-controlled process.

Karlsson et al. (1999) then went on to derive the spherical particle diameter that would be required to achieve a penetration depth of less than the 50 μm quoted from Holgersson et al. (1998).

The particle diameter that was derived using this method was found to be around 6 mm, which has a spherical area to volume ratio of 960 m^{-1}. This is close to the minimum size of the 4-32 mm diameter particles proposed in the sand/gravel backfill. The average particle (by volume) of the proposed sizes has a diameter of 25 mm, which has a spherical area to volume ratio of 240 m^{-1} (it was noted in Section 2 that this is not necessarily a good average to use and that a better approximation could be made, based on the distribution of particle sizes). Thus the area to volume ratio of the average particle in the backfill was found to be too small to sustain a required penetration depth of less than 50 μm. However, Karlsson et al. (1999) then went on to argue that spherical area to volume ratios generally under-predict area to volume ratios when compared to BET data, and claim that the actual surface area is probably between 125 and 200 times larger than the estimated spherical surface area. This would give an area to volume ratio of between 30 000 and 50 000 m^{-1} for the average diameter particle, which would then be sufficient to maintain the requirement that the penetration depth

were less than 50 μm. However, in making this calculation, Karlsson et al. (1999) implicitly assume that almost the entire volume of the particle is accessible within the 50 μm depth.

The key point to note about all of the preceding argument is that it is based entirely on the assumption that there is a "penetration depth", s, within the particle (e.g. *Figure 1a*). This assumption has been addressed by carrying out particle-scale calculations with *Raiden2*, discussed in detail, below. However, as described by Holgersson et al. (1998), it is much more likely that the reaction of the particles is a surface process and solid alteration products accumulate on the surface of the particles only (*Figure 1b*).

3.2.1 Model input considerations

A 1-D radially-symmetrical particle model[1] was set up in *Raiden2* to represent the idealised spherical particle (*Figure 2*). Along the modelled dimension, nodes were placed, with the node density being highest near the particle boundary, in an attempt to capture behaviour at the 50 μm scale (*Table 2*). A particle diameter of 18 mm was assumed in the model. This is smaller than the average size (by diameter) of particles considered by Karlsson et al. (1999), but is probably a better representation of the true average particle size in the backfill if the size range is 4 – 32 mm (Section 2). The reference temperature in the model was set to 25 ºC. The pore water boundary condition on the outside of the particle was taken to be Dirichlet (fixed) at the cement water concentrations; a Neumann (zero flux) boundary condition was assumed on the inner boundary.

Two cement water compositions were used as boundary conditions in the modelling. The first, was derived by equilibrating portlandite, $Ca(OH)_2$ with pure water at 25 °C

[1] *Raiden2* is capable of modelling systems in one or two spatial dimensions using non-uniform grids in Cartesian or cylindrical-polar coordinates. For the particle scale modelling, the most applicable geometry would be a three dimensional spherical-polar coordinate, but since this feature is not currently available in *Raiden2*, two-dimensional cylindrical-polar coordinates have been used instead. Such an approximation would be expected to slightly under-predict the flux of aqueous species in the pore space, but for shallow penetration depths, the effect is likely to be small.

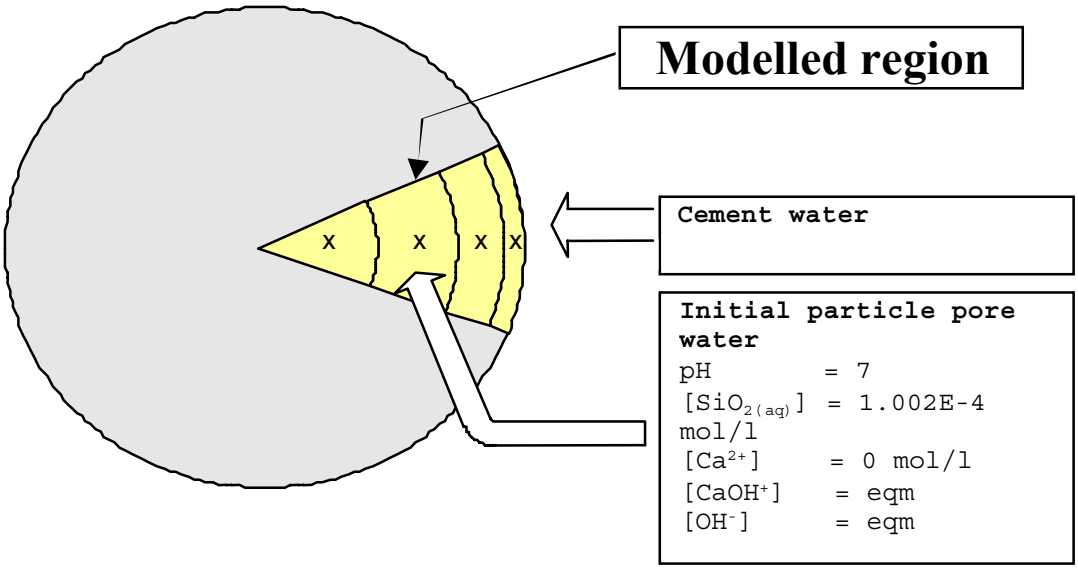

Figure 2 Idealised 1-D radially symmetrical geometry assumed for the Raiden2 modelling.

Table 2 Cells/nodes used in the particle interior modelling.

Cell Boundaries (from particle centre)	Node positions (from particle centre)	Depth of region (from particle surface)
1.000E-03 m (Interior boundary)		
	2.500E-03 m	5-8 mm
4.000E-03 m		
	5.000E-03 m	3-5 mm
6.000E-03 m		
	7.000E-03 m	1-3 mm
8.000E-03 m		
	8.250E-03 m	0.5-1 mm
8.500E-03 m		
	8.700E-03 m	0.1-0.5 mm
8.900E-03 m		
	8.913E-03 m	75-100 μm
8.925E-03 m		
	8.938E-03 m	50-75 μm
8.950E-03 m		
	8.963E-03 m	25-50 μm
8.975E-03 m		
	8.988E-03 m	0-25 μm
9.000E-03 m (Cement water boundary)		

using the *Geochemist's Workbench* computer code (Bethke, 1996). The results of this calculation are shown in *Table 3*.

The second cement pore water composition is that quoted by Holgersson et al. (1998) [*Table 4*]. This reference is used by Karlsson et al. (1999) when attempting to justify the amount of cement water buffering that is possible by a single backfill particle. This water has a higher $SiO_{2(aq)}$ content than that shown in *Table 3*.

The initial pore water in the backfill particle is assumed to be in equilibrium with quartz at neutral pH. The composition is shown in *Table 5*.

Transport within the particle is assumed to be purely diffusive. There was no applied flow, but porosity changes within the particle could give rise to small fluxes in the particle pore water. The diffusion coefficients for the aqueous species in the model are given in *Table 6*.

The backfill particles were assumed to be composed entirely of quartz. This is inconsistent with the backfill envisaged for SFL 3-5, which will contain around 30 % quartz (typical 'granite' [*sensu lato*] composition), but is consistent with the assumptions made by Karlsson et al. (1999) as was discussed in Section 2 of this report. The reason for making the assumption here is so that the results presented here can be compared with those of Karlsson et al. (1999).

For the set of simulations performed in this modelling exercise, three models for quartz dissolution have been used. The first model, assumed to be the base case, is that described in Knauss and Wolery (1988). These authors describe a quartz dissolution reaction mechanism that is a function of pH, which was derived from a suite of experiments that were performed at 70 ºC. Knauss and Wolery (1988) also extrapolate their results to 25 °C, and these results are used in this modelling exercise. This reaction estimate was also used by Karlsson et al. (1999) to derive a release rate of $SiO_{2(aq)}$ from granite particles.

Table 3 Base case cement water composition.

Porewater basis species	Concentration (mol/l)
H^+	4.28×10^{-13}
Ca^{2+}	1.30×10^{-2}
$SiO_{2(aq)}$	1.00×10^{-36}

Table 4 Cement water composition used by Holgersson et al. (1998).

Porewater basis species	Concentration (mol/l)
H^+	1.00×10^{-13}
Ca^{2+}	2.5×10^{-3}
$SiO_{2(aq)}$	4.5×10^{-5}

Table 5 Initial pore water composition.

Porewater basis species	Concentration (mol/l)
H^+	1.00×10^{-7}
Ca^{2+}	1.00×10^{-30}
$SiO_{2(aq)}$	1.00×10^{-4}

Table 6 Diffusion coefficients used in the particle scale modelling.

Aqueous Species	Diffusion coefficient (m^2/s)
H^+	4×10^{-14}
All other species	1×10^{-13}

The second dissolution model for quartz is that quoted by Savage et al. (1992), which is a reaction mechanism that is a function of pH, but which is calculated at 70 °C. Being at a higher temperature, this reaction has a much faster rate than that that calculated at 25 °C by Knauss and Wolery (1988), which will thus provide an insight into the variation of reaction depth with the speed of release of aqueous silica into the pore water in the particle, since it may be anticipated that a faster dissolution of quartz would lead to an enhanced pH buffering capacity in the backfill.

The final dissolution model for quartz is that described by Rimstidt and Barnes (1980). This reaction mechanism was derived as a function of temperature at fixed (neutral) pH. This reaction mechanism is the slowest of the three considered here and is included so that the effect of a slower quartz reaction can be seen.

The form of the pH dependent reaction used by both Knauss and Wolery (1988) and Savage et al. (1992) is:

$$\frac{dm_{quartz}}{dt} = A_{quartz} k\left(\mathrm{H}^{+}\right)\left(\frac{Q_{quartz}}{K_{quartz}} - 1\right) \tag{19}$$

Here, A_{quartz} is the surface area of quartz per unit volume (m^2/m^3), and is given by:

$$A_{quartz} = A^{sp}_{quartz} \times W^{mol}_{quartz} \times m_{quartz} \tag{20}$$

where A^{sp}_{quartz} is the specific surface area (m^2/g) and W^{mol}_{quartz} is the molar weight (g/mol) of quartz. For the purpose of this modelling, A_{quartz} was taken to be 2.27 m^2/g.

The reaction rates for the three quartz reactions are shown graphically in *Figure 3*. For temperatures close to 0 °C, Rimstidt and Barnes' expression for the rate constant tends to slightly over-predict the equilibrium constants for quartz hydrolysis in the EQ3/6 database, which means that at these low temperatures, quartz will dissolve at higher

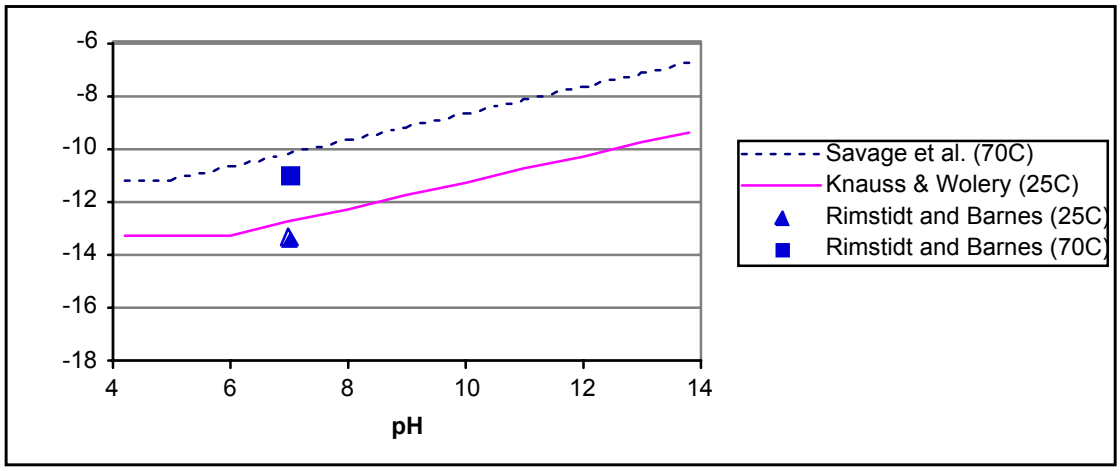

Figure 3 Log rates of quartz dissolution as a function of pH and temperature.

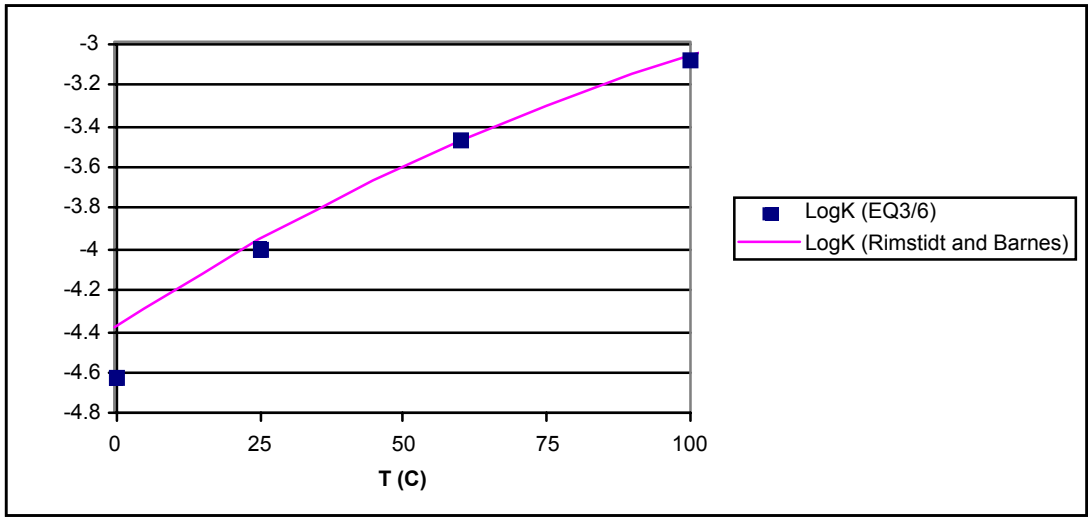

Figure 4 Temperature dependent equilibrium constants. Knauss and Wolery (1988) and Savage et al. (1992) reactions use the EQ3/6 value of log K, whereas the Rimstidt and Barnes (1980) reaction uses an analytical temperature dependency.

Table 7 Candidate CSH phases included in particle-scale modelling.

Candidate CSH phase	Hydrolysis reaction		
Hillebrandite	$Ca_2SiO_3(OH)_2{:}0.17H_2O + 4H^+$	=	$SiO_{2(aq)} + 2Ca^{2+} + 3.17H_2O$
Afwillite	$Ca_3Si_2O_4(OH)_6 + 6H^+$	=	$2SiO_{2(aq)} + 3Ca^{2+} + 6H_2O$
Foshagite	$Ca_4Si_3O_9(OH)_2{:}0.5H_2O + 8H^+$	=	$3SiO_{2(aq)} + 4Ca^{2+} + 5.5H_2O$
Xonotlite	$Ca_6Si_6O_{17}(OH)_2 + 12H^+$	=	$6SiO_{2(aq)} + 6Ca^{2+} + 7H_2O$
Tobermorite-14A	$Ca_5Si_6H_{21}O_{27.5} + 10H^+$	=	$6SiO_{2(aq)} + 5Ca^{2+} + 15.5H_2O$
Gyrolite	$Ca_2Si_3O_7(OH)_2{:}1.5H_2O + 4H^+$	=	$3SiO_{2(aq)} + 2Ca^{2+} + 4.5H_2O$
Okenite	$CaSi_2O_4(OH)_2{:}H_2O + 2H^+$	=	$2SiO_{2(aq)} + Ca^{2+} + 3H_2O$

SiO_2 activities than would be predicted by reactions based on the equilibrium constant of the EQ3/6 database. However, at the reference temperature of 25 °C, the agreement between the two equilibrium constants is good, with a difference in log K of approximately 1 %. The log K values for quartz hydrolysis from EQ3/6 and Rimstidt and Barnes are compared in *Figure 4*.

In order to analyse the composition of the alteration layer, rather than represent the alteration layer as a single CSH phase (as in Karlsson et al., 1999), several potential CSH phase candidates were included in the model. The candidate CSH phases and their properties are listed in *Table 7*.

No data were available for the rate of growth of any of the secondary minerals, so the initial *Raiden2* modelling that was performed assumed instantaneous equilibrium reactions for each of the secondary minerals.

The assumption of instantaneous equilibrium reactions imposes an extra burden on the computer code and leads to longer solution times, so following some initial exploratory *Raiden2* simulations the instantaneous equilibrium reactions were replaced with a set of fast kinetic reactions that were found to be sufficiently fast that the results obtained were indistinguishable from the instantaneous equilibrium results. The kinetic reaction that was used for each of the CSH phases was

$$\frac{dm_i}{dt} = A_{M_i} k_{fast} \left(\frac{Q_{M_i}}{K_{M_i}} - 1 \right) \tag{21}$$

Here, A_{M_i} is the surface area of the i^{th} mineral, and is given by

$$A_{M_i} = A_{M_i}^{sp} \times W_{M_i}^{mol} \times m_i \tag{22}$$

where $A_{M_i}^{sp}$ is the specific surface area (m^2/g) and $W_{M_i}^{mol}$ is the molar weight (g/mol) of the i^{th} mineral, and k_{fast} was taken to be 10^2 mol m^{-2} y^{-1}. The resulting reaction rate is therefore significantly faster than the rate of quartz dissolution using the Knauss and Wolery reaction (1988) that is being used as the ”base case” reaction, and is approximately an order of magnitude faster than the fast quartz dissolution rate from Savage et al. (1992) at pH 14 and is approximately two orders of magnitude faster at pH 12, which is closer to the highest pH observed in most of the simulations. Since we are approximating an instantaneous reaction with a kinetic reaction, an accurate value for the surface area term is unnecessary (provided that the value assumed is at least as large as the specific surface area in the quartz reaction) since this value only acts to scale the reaction rate. Hence the specific surface area of all of the CSH phases was assumed tobe equal to that assumed for quartz, 2.27 m^2/g.

Figure 5 shows log (*Q/K*) for the tobermorite phase in a single cell with this fast kinetic reaction mechanism. Tobermorite begins to precipitate at around 10^{-5} years (i.e. almost immediately) when log (*Q/K*) approaches zero, after which time the fast reaction rate maintains log (*Q/K*) close to zero. A summary of the reactions equations used for the minerals in the *Raiden2* modelling, together with the appropriate parameter values, is given in *Table 8.*

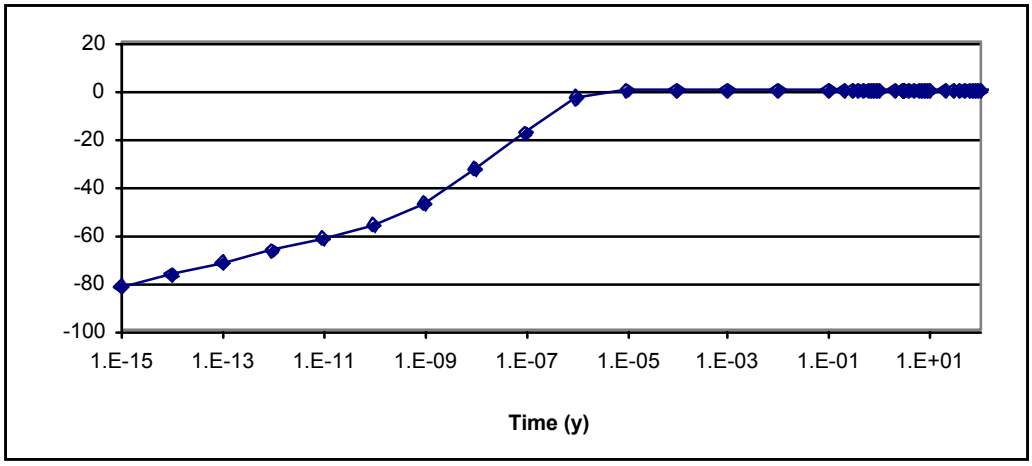

Figure 5 Log (Q/K) for the tobermorite phase using the fast kinetic reaction. Tobermorite is initially under saturated and once saturated is held close to equilibrium.

Three kinetic reaction mechanisms for quartz were considered – the Knauss and Wolery reaction (the base case), the faster Savage et al. reaction and the slower Rimstidt and Barnes reaction, together with two possible cement waters, one with a low Si content and one with a high Si content. This gives a potential six simulations to run. However since one of the potential models is assumed to be the base case model (the Knauss and Wolery reaction and the low Si content cement water), only four simulation have been considered, which correspond to single perturbations of the base case model (i.e. not perturbing both the quartz reaction and the cement water), as described in *Table 9.*

The other two variants of the base case have not been considered since the inclusion of the faster and slower quartz reactions is only intended to demonstrate the effect of including a significantly altered quartz dissolution reaction, and so it has not been included with regard to the presence of the high silica content cement water.

Table 8 Reaction equations used in the Raiden2 particle-scale modelling.

[1]Non temperature-dependent values taken from EQ3/6 database.

Mineral		**Log k (mol m^{-2} s^{-1})**	**Log K[(1)] (at 25°C unless indicated otherwise)**	**A^{sp} (m^2/g)**	**V^{mol} [(1)] (m^3/mol)**	**W^{mol} [(1)] (g/mol)**
Quartz	$Ak(\mathrm{H}^+)\left(\frac{Q}{K}-1\right)$ (Knauss and Wolery, 1988)		-3.9993	2.27	2.27×10^{-5}	60.08
	$Ak(\mathrm{H}^+)\left(\frac{Q}{K}-1\right)$ (Savage et al., 1992)		-3.9993	2.27	2.27×10^{-5}	60.08
	$Ak_{rb}(\mathrm{T})\left(\frac{Q}{K_{rb}(T)}-1\right)$ (Rimstidt and Barnes, 1980)	$1.174 - 2.028\times10^{-3}\mathrm{T} - 4158/\mathrm{T}$	$1.881 - 2.028\times10^{-3}\mathrm{T} - 1560/\mathrm{T}$	2.27	2.27×10^{-5}	60.08
Hillebrandite	$Ak_{fast}\left(\frac{Q}{K}-1\right)$	3.171×10^{-6}	36.8190	2.27 [(2)]	7.18×10^{-5}	193.32
Afwillite	*as above*	3.171×10^{-6}	60.0452	2.27 [(2)]	1.29×10^{-4}	342.45
Foshagite	*as above*	3.171×10^{-6}	65.9210	2.27 [(2)]	1.54×10^{-4}	431.59
Xonotlite	*as above*	3.171×10^{-6}	91.8267	2.27 [(2)]	2.65×10^{-4}	714.99
Tobermorite	*as above*	3.171×10^{-6}	63.8445	2.27 [(2)]	2.87×10^{-4}	739.98
Gyrolite	*as above*	3.171×10^{-6}	22.9099	2.27 [(2)]	1.37×10^{-4}	337.45
Okenite	*as above*	3.171×10^{-6}	22.9099	2.27 [(1)]	9.48×10^{-5}	212.28

[2]Value is arbitrary (provided that it is sufficiently large) since an instantaneous reaction is being approximated

Table 9 Model scenarios considered in the modelling exercise.

Quartz reaction	**Base cement water (low Si)**	**Holgersson et al. cement water (high Si)**
Knauss and Wolery reaction (base case)	✓	✓
Savage et al. reaction	✓	×
Rimstidt and Barnes reaction	✓	×

3.2.2 Results

For each case considered, the simulation was run for 50 (simulated) years. Outputs from the modelling include:

- Total concentrations of SiO_2, Ca^{2+} and OH^- in the particle (in both the pore water and minerals).
- Concentrations of each of the mineral species for each cell in the model.
- Concentrations of each of the aqueous species for each cell in the model.
- The porosity in each cell in the mode.

Base case

Results from these simulations are shown in *Figures 6-8.* The first key output of the modelling is that the total SiO_2 content in the particle remains essentially unchanged for the entire evolution (the loss after 50 years is only 10^{-5} % of the initial total), so that all SiO_2 initially in the particle in either the pore water or quartz remains in the particle, albeit possibly in a CSH phase. The implication of this is that the only SiO_2 that is available for reaction is either on the surface of, or outside the particle. Thus no SiO_2 escapes from the interior of the particle to take part in the buffering reaction on the particle surface or nearby in the backfill pore space.

The second key result is that the outermost cell in the model (that which models the region in the particle from the surface to a depth of 25 μm) becomes entirely blocked with precipitate after approximately 1 year, the dominant precipitate being a gyrolite phase. Prior to this time, a tobermorite phase had precipitated in the pore space in the outermost cell following the increase in Ca concentration and pH as the cement water began to diffuse into the particle. The tobermorite phase subsequently dissolved as the pore water chemistry became more favourable for gyrolite precipitation following further cement water intrusion. A small amount of tobermorite is re-precipitated after 1 year following a small amount of sacrificial gyrolite dissolution in the blocked cell, the resulting CSH phase at 50 years being around 99 % gyrolite and 1 % tobermorite.

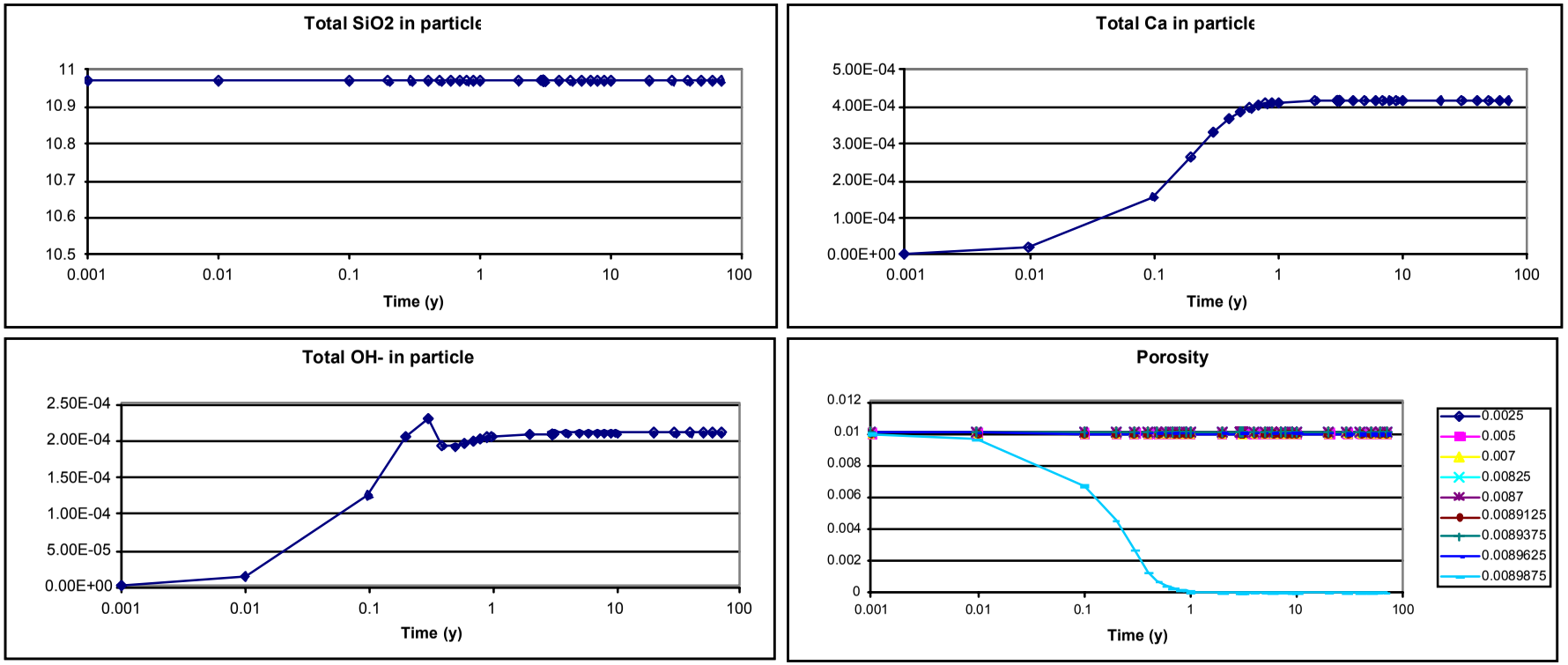

Figure 6 Base case: Evolution of total Si, Ca and OH and porosity in the particle. The colour data points refer to different nodes within the particle, ranging from 0.0025 to 0.0089875 m from the particle centre.

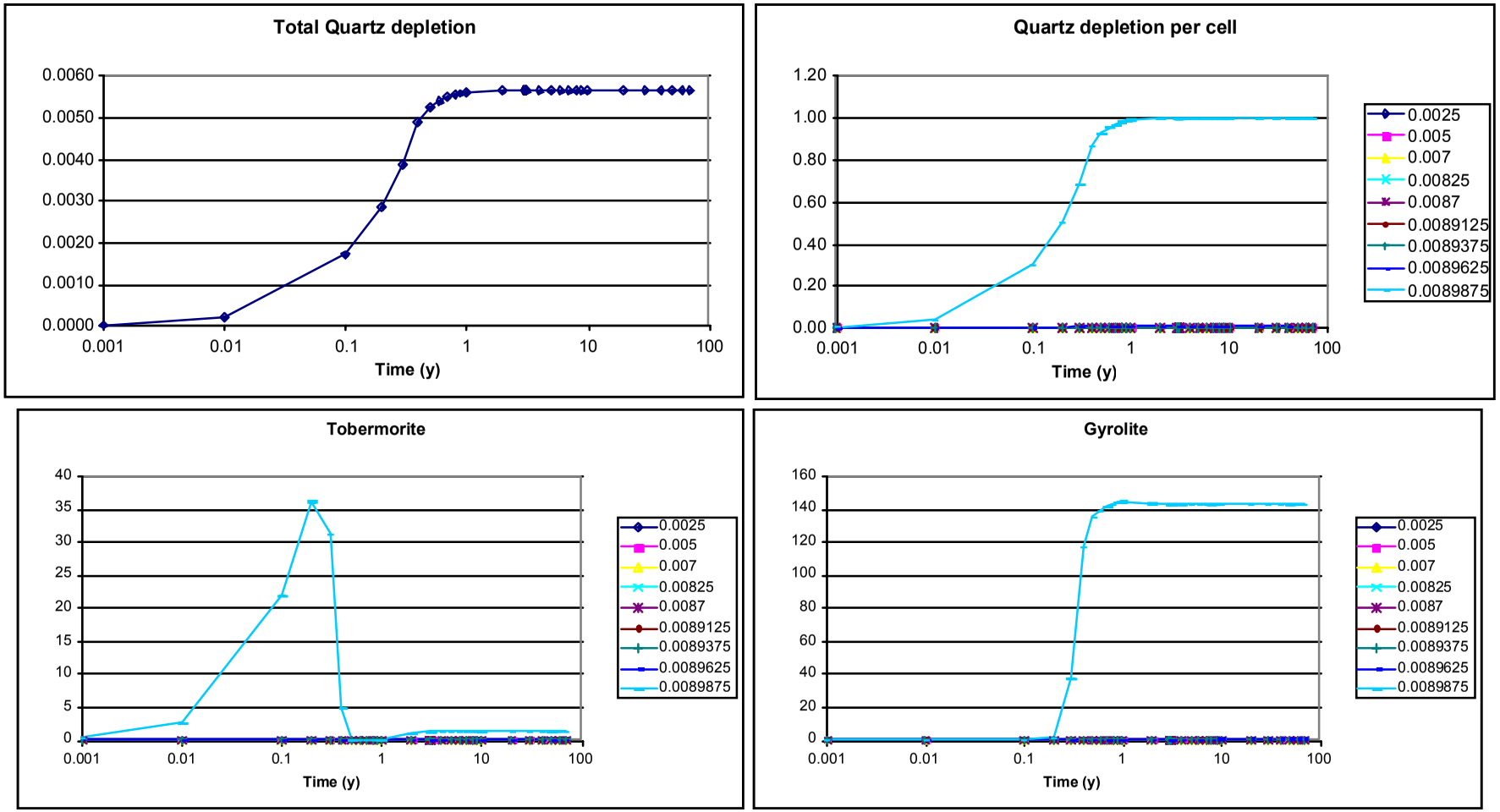

Figure 7 Base case: Evolution of quartz and CSH in the particle. The colour data points refer to different nodes within the particle, ranging from 0.0025 to 0.0089875 m from the particle centre.

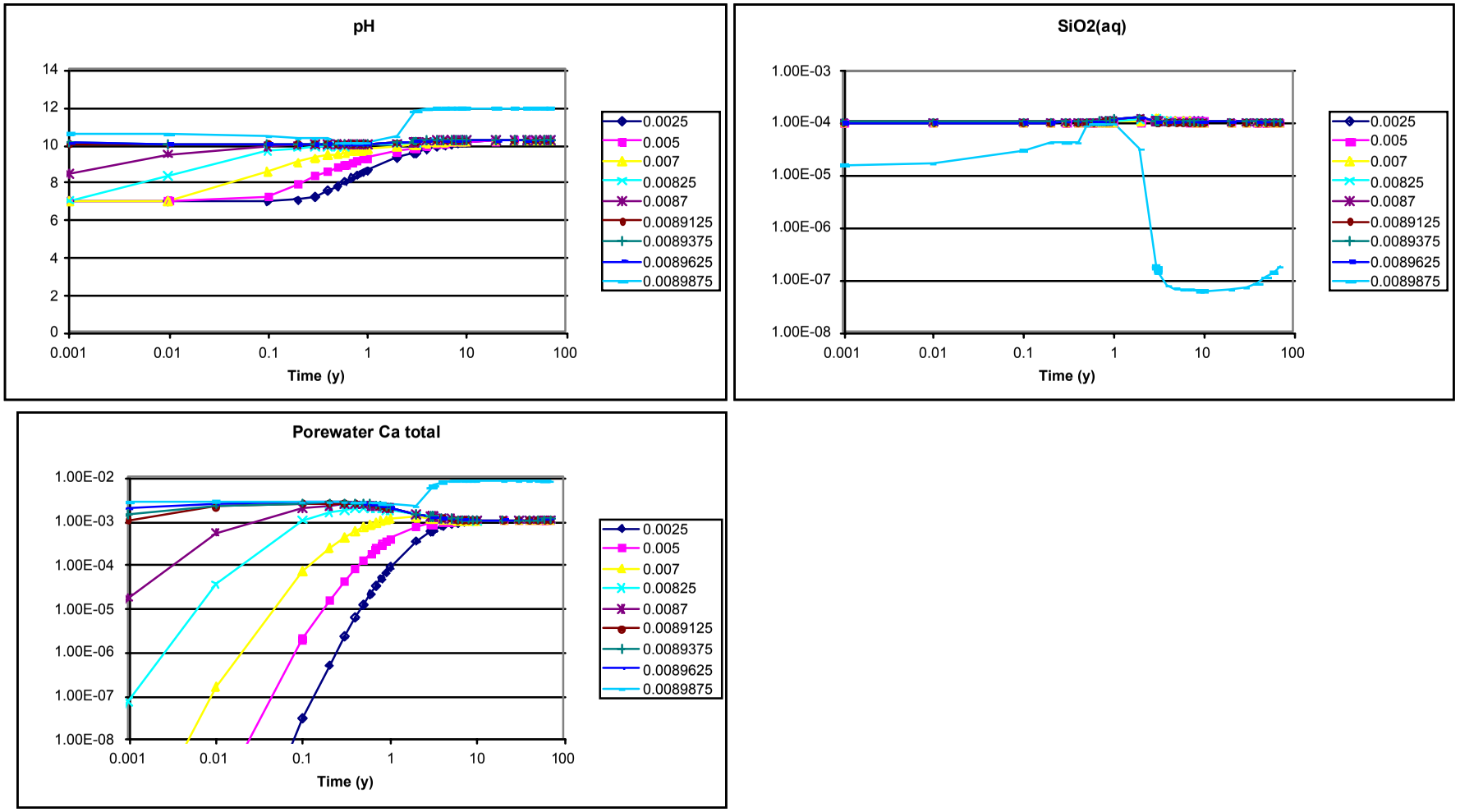

Figure 8 Base case: Evolution of pH, Ca, and SiO_2 in the particle pore water. The colour data points refer to different nodes within the particle, ranging from 0.0025 to 0.0089875 m from the particle centre.

The blocking of the particle to a depth of 25 μm lowers the porosity to almost zero (< 0.01 % porosity remains in the model in an effort to simulate transport through imperfections in the precipitated phases that permit a small amount of through-diffusion), which effectively shields the remainder of the interior of the particle at depths greater than 25 μm from the cement water. All further transport of pore water species between the cement water and the particle interior has to pass through the blocked cell, hence the rate at which the particle continues to undergo geochemical alteration is greatly reduced. At the end of the 50-year simulation, the concentration of gyrolite in the cell neighbouring the blocked cell is only 1 % of the concentration in the blocked cell due to the long transport time through the blocked cell. The concentration of gyrolite in the next cell again is 10^{-6} of that in the blocked cell.

The pore water inside the particle that is shielded from the cement water by the blocked cell remains close to equilibrium with quartz, so very little quartz dissolution takes place at depth within the particle. The only significant dissolution of quartz is in the outermost cell before it becomes blocked, where approximately 1 % of the quartz dissolves before the cell becomes blocked. By approximately 10 years the pH in the particle is fairly uniform around 10, except in the blocked cell where the (trivial amount of) pore water has pH around 12.

In summary, very little alteration of the particle is observed at depth due to the rapid blocking of the outer pore space of the particle with a predominantly gyrolite CSH phase, and very little SiO_2 escapes from the interior of the particle to react on the surface of the particle or in the pore water close to the surface of the particle.

The observations here contrast with those in Karlsson et al. (1999), where a ”penetration depth” of 50 μm in which total conversion of quartz to CSH was assumed.

High Si content cement water

The results obtained when perturbing the base case to assume the high Si content cement water boundary condition are plotted in *Figures 9-11*.

The results are very similar to those in the base case modelling. Again the outermost cell, representing the region in the particle from the surface to a depth of 25 μm becomes blocked by a CSH phase which effectively shields the interior of the particle from further cement water intrusion, other than the slow intrusion through the trivial pore space in the blocked cell. The time taken for the pore space to block is around 3 years in this case compared to 1 year in the base case. The delay is due to the Si rich cement water causing a less dramatic reduction in Si content as pore water diffuses out of the particle compared to the base case where the Si content in the cement water was lower. The resulting increased Si content over that in the base case in the outermost cell causes the rate of quartz dissolution to be smaller as the pore water is closer to equilibrium with quartz than was the case in the base case, and hence a slower rate of release of SiO_2 from the particle with which to precipitate the CSH layer. A small amount of tobermorite precipitates after a small amount of sacrificial dissolution of gyrolite has occurred. The resulting CSH layer is calculated to be 99.8 % gyrolite and 0.2 % tobermorite.

The total amounts of quartz dissolved show only a fractional increase over those in the base case. The amount of OH^- "consumed" by the particle is approximately 50 % greater than that in the base case; the extra OH^- being held in the particle pore water at depth, behind the shielding CSH layer, due to the greater time available for the diffusion of cement water into the particle to occur before the outer pore space becomes blocked. This leads to an increased pH at depth in the particle to 12.7 from the base case where pH was around 10.2. This increased pH does not lead to any significant quartz dissolution however, as there is sufficient Si in the pore water due to its equilibration with quartz.

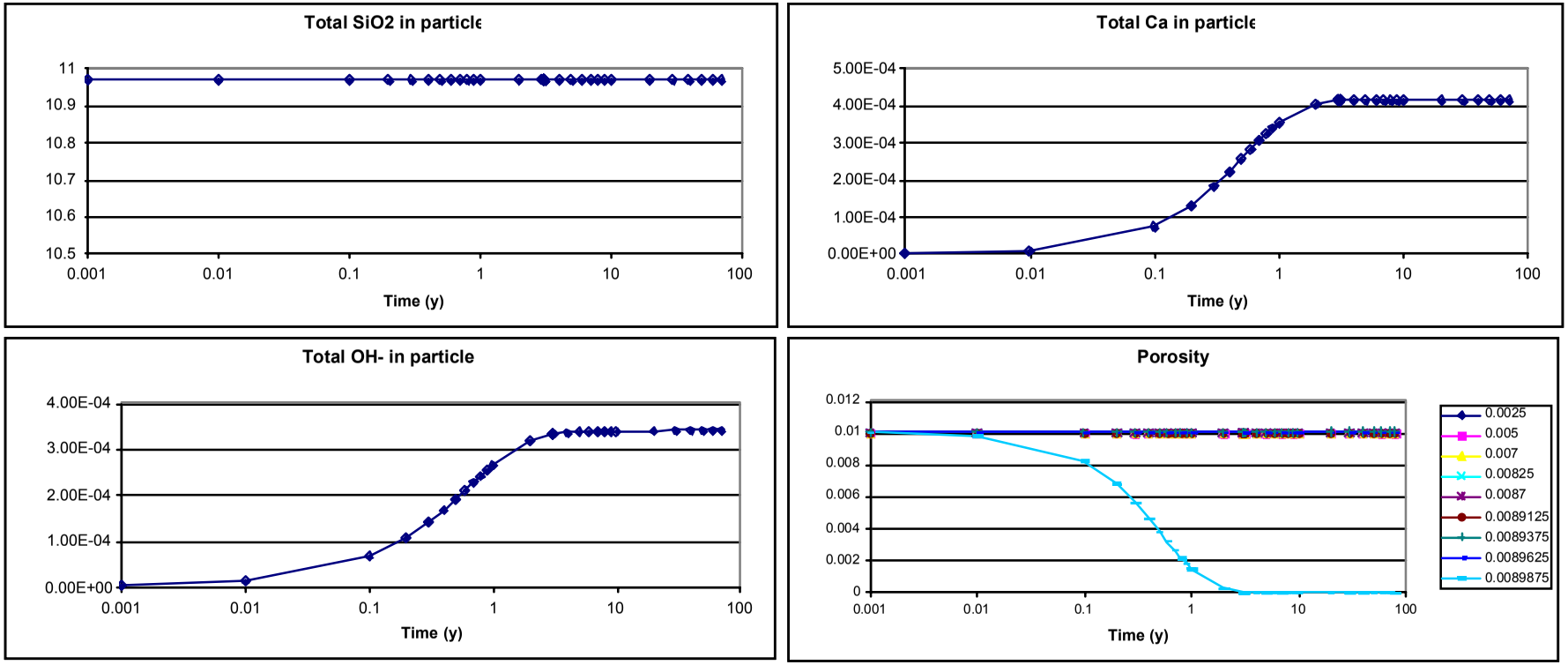

Figure 9 High Si cement water case: Evolution of total Si, Ca and OH⁻ and porosity in the particle. The colour data points refer to different nodes within the particle, ranging from 0.0025 to 0.0089875 m from the particle centre.

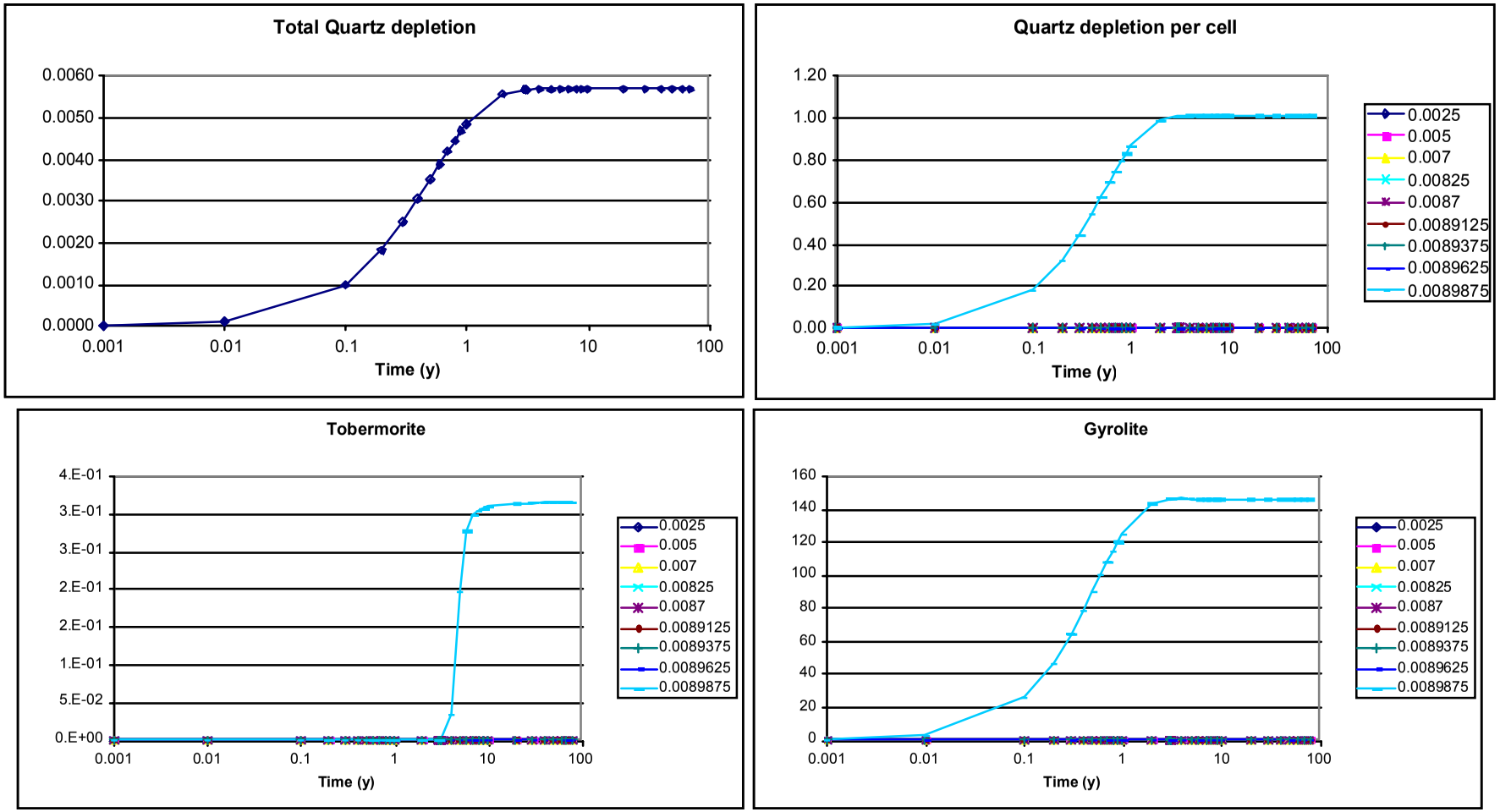

Figure 10 High Si cement water case: Evolution of quartz and CSH in the particle. The colour data points refer to different nodes within the particle, ranging from 0.0025 to 0.0089875 m from the particle centre.

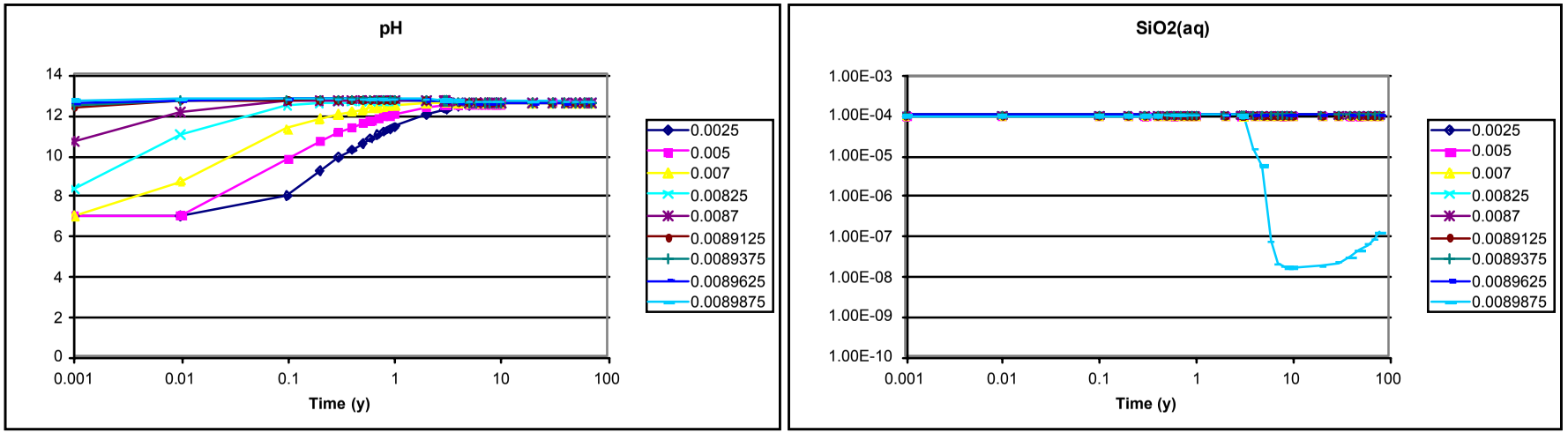

Figure 11 High Si cement water case: Evolution of pH, SiO_2 in the particle pore water. The colour data points refer to different nodes within the particle, ranging from 0.0025 to 0.0089875 m from the particle centre.

Fast quartz dissolution

The results obtained when perturbing the base case to assume the fast quartz dissolution data of Savage et al. (1992) derived at 70 °C are plotted in *Figures 12-14*.

The results after 50 years are almost exactly the same as the base case results. Once again, the pore space becomes blocked with precipitated CSH to a depth of 25 μm after approximately 1 year. The CSH phase is predominantly gyrolite, together with a small (< 0.02 %) amount of tobermorite. The gyrolite phase begins to precipitate earlier than in the base case in response to the increased amount of Si in the pore water due to the faster rate at which quartz is dissolved.

Slightly more quartz depletion is observed in the outermost cell before it becomes blocked with precipitate, but the amount is still trivial (around 1 % in the outermost cell, and less than 0.006 % overall).

The total amount of OH^- ”consumed” by the particle is similar to that in the base case and so the pH profile in the particle mirrors that in the base case.

In summary, the blockage of the outermost pore space shields the remainder of the interior of the particle so that the effect of the enhanced quartz dissolution rate over that in the base case goes unnoticed.

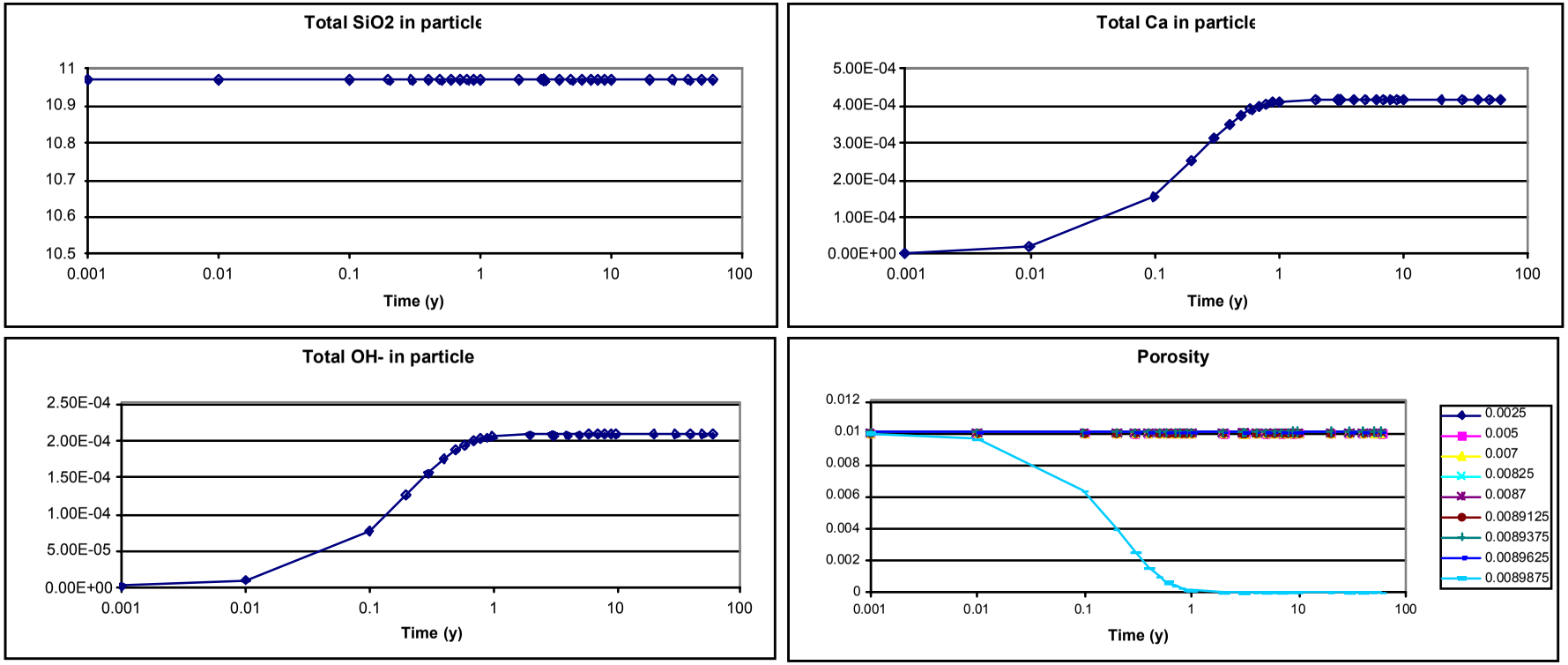

Figure 12 Fast quartz dissolution case: Evolution of total Si, Ca and OH^- and porosity in the particle. The colour data points refer to different nodes within the particle, ranging from 0.0025 to 0.0089875 m from the particle centre.

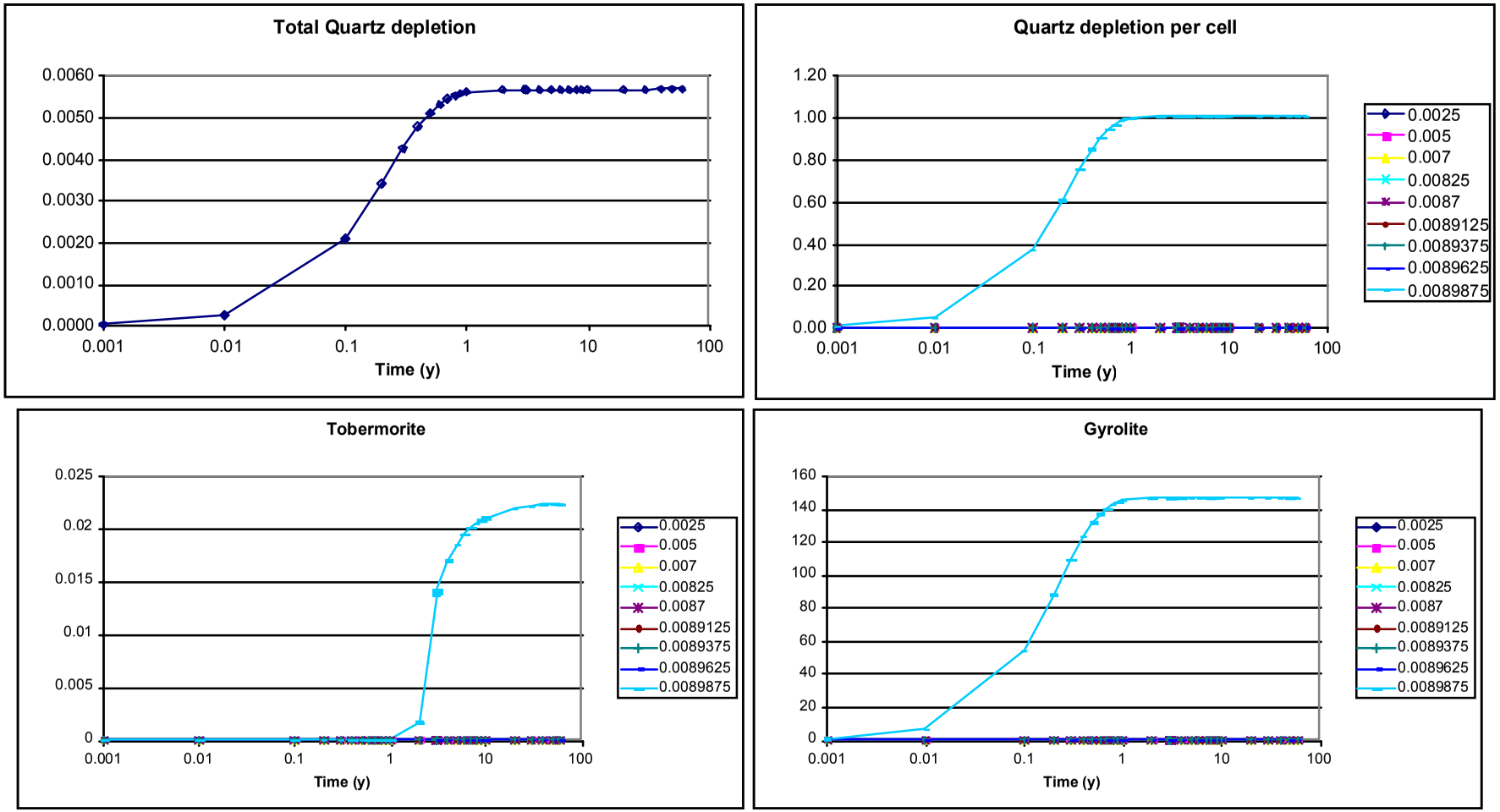

Figure 13 Fast quartz dissolution case: Evolution of quartz and CSH in the particle. The colour data points refer to different nodes within the particle, ranging from 0.0025 to 0.0089875 m from the particle centre.

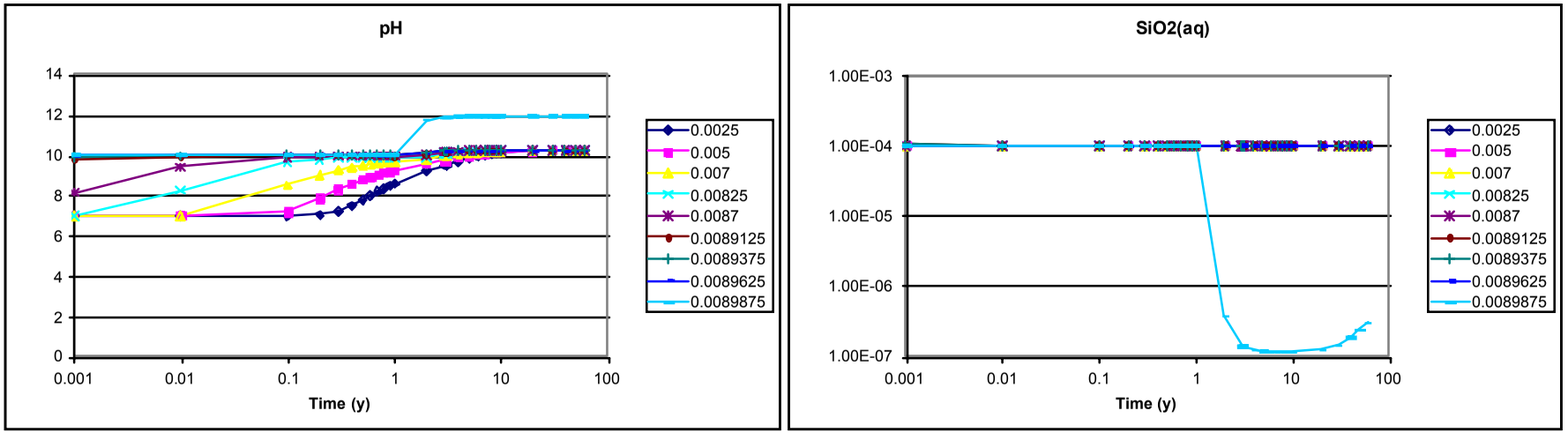

Figure 14 Fast quartz dissolution case: Evolution of pH and SiO_2 in the particle pore water. The colour data points refer to different nodes within the particle, ranging from 0.0025 to 0.0089875 m from the particle centre.

Slow quartz dissolution

The results obtained when perturbing the base case to assume the slow quartz dissolution reaction of Rimstidt and Barnes (1980) are plotted in *Figures 15-17.*

The results in this case display the greatest difference from the base case results of all of the particle interior models. It is still the case that the total Si content of the particle is unchanged, so that no Si that is initially in the interior of the particle escapes to take part in reactions on the particle surface or nearby in the particle pore water. However, the evolution of the particle is somewhat different, as described below.

As was the case in the base case modelling, the interior of the particle becomes blocked with precipitate. However, in this case the blocking occurs at around 50 years in all of the outermost 4 cells, corresponding to the region in the particle from the surface to a depth of 100 μm. The reason for the greater depth and slower rate of blocking is that the slower quartz dissolution reaction supplied Si to the pore water at a rate that is much slower than the rate at which Si diffuses out of the particle. Therefore prior to blocking, the Si content in the pore water in the outermost cells is significantly lower than the base case. The pore water there can only become saturated with respect to one of the CSH phases once sufficient Ca^{2+} and OH^- has diffused into the particle, and so the onset of CSH precipitation is delayed. Once the pore water becomes saturated with respect to a CSH phase, the CSH will only precipitate at a rate close to that at which Si is released to the pore water from the quartz. The combination of the slower reaction rate of the Rimstidt and Barnes reaction and the greater distance of the pore water from equilibrium with quartz results in a dissolution rate that is around 2 orders of magnitude slower than in the base case. The pore space therefore closes more slowly, allowing more time for in diffusion of the cement water and hence greater penetration of the cement water into the particle. Each of the four outermost cells (which are all small, having a depth of 25 μm) evolves at a similar rate, so that the graphs of the evolution in each cell are virtually indistinguishable.

Due to the resulting pore water in the particle varying from that in the base case (there is less Si and more Ca^{2+} and OH^- ions), tobermorite is the dominant CSH phase in the blocked region to a depth of 100 μm. Beyond the blocked region, the next cell which

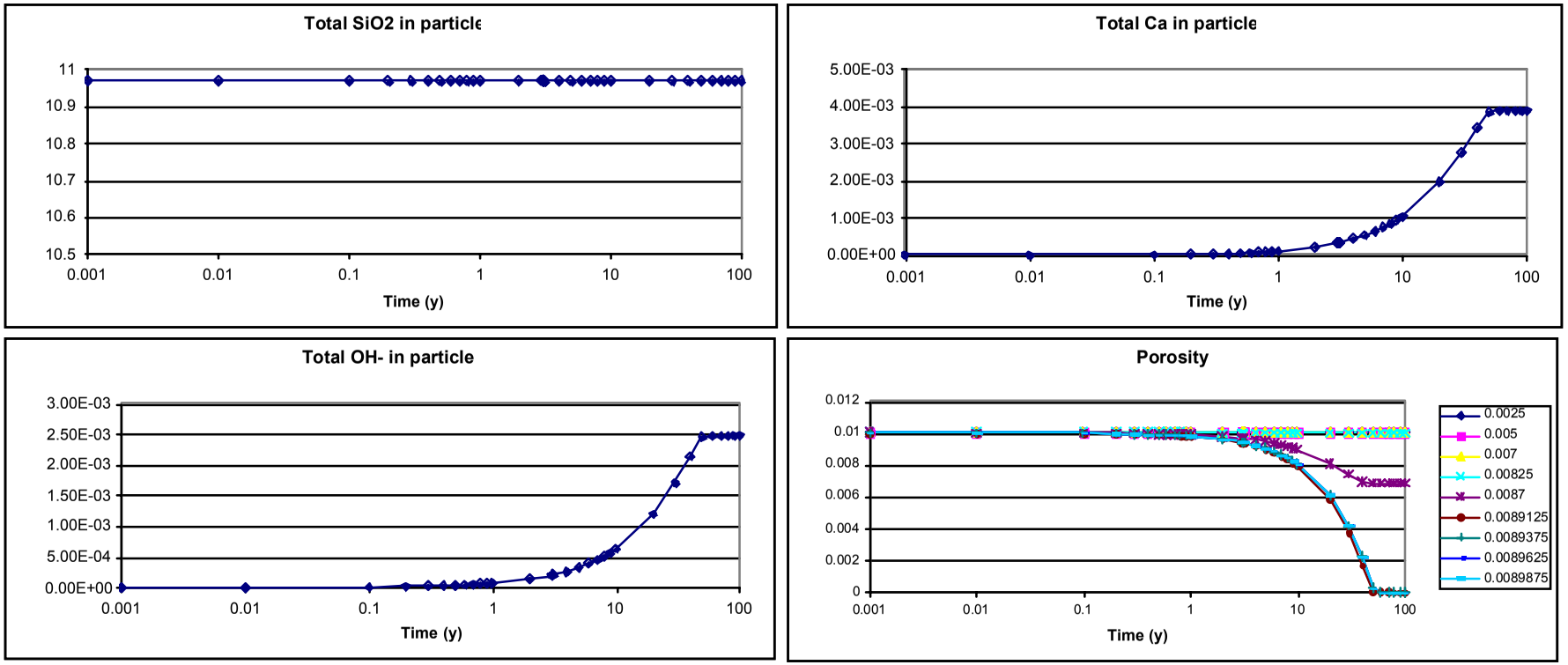

Figure 15 Slow quartz dissolution case: Evolution of total Si, Ca and OH and porosity in the particle. The colour data points refer to different nodes within the particle, ranging from 0.0025 to 0.0089875 m from the particle centre.

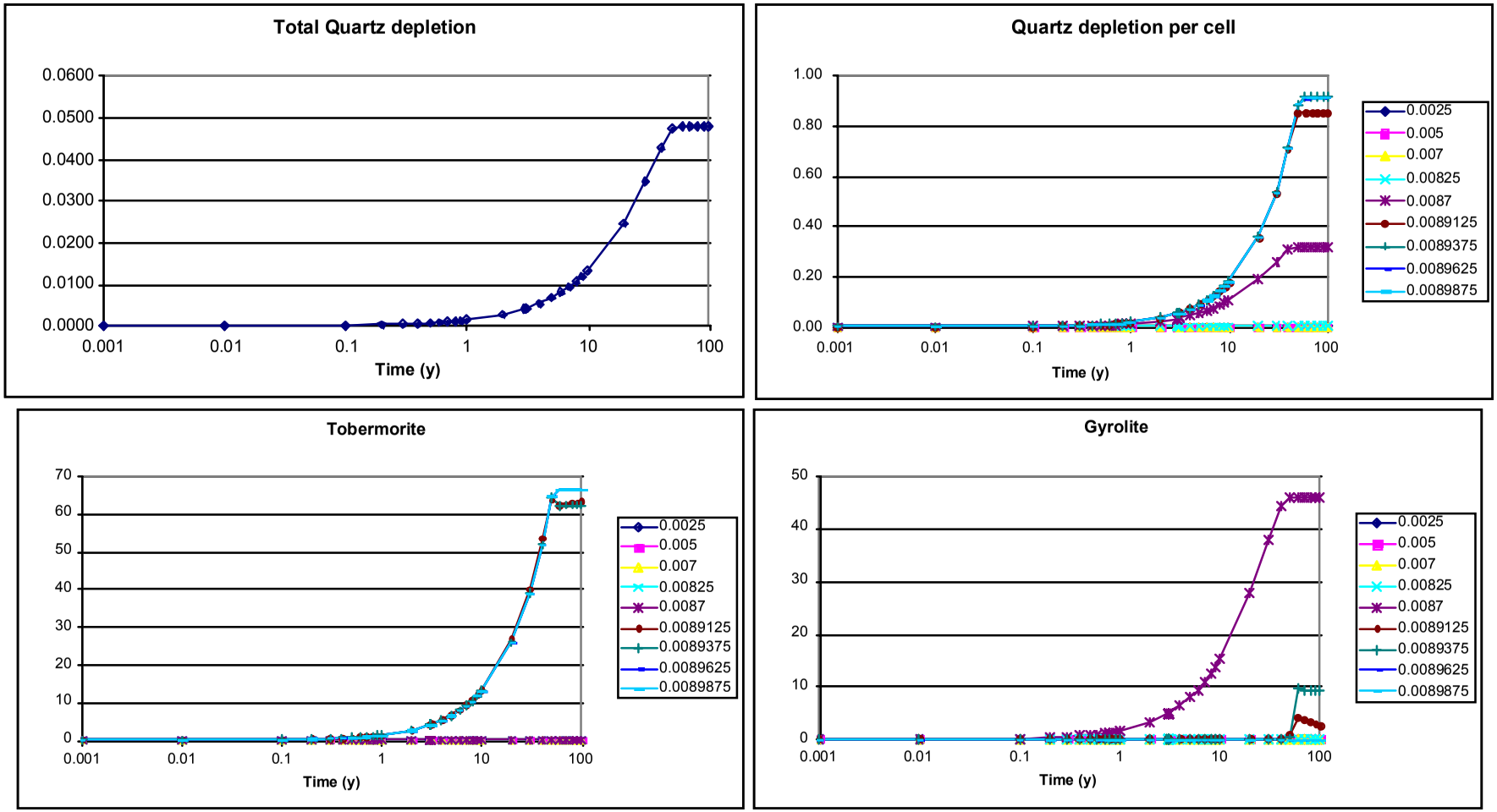

Figure 16 Slow quartz dissolution case: Evolution of quartz and CSH in the particle. The colour data points refer to different nodes within the particle, ranging from 0.0025 to 0.0089875 m from the particle centre.

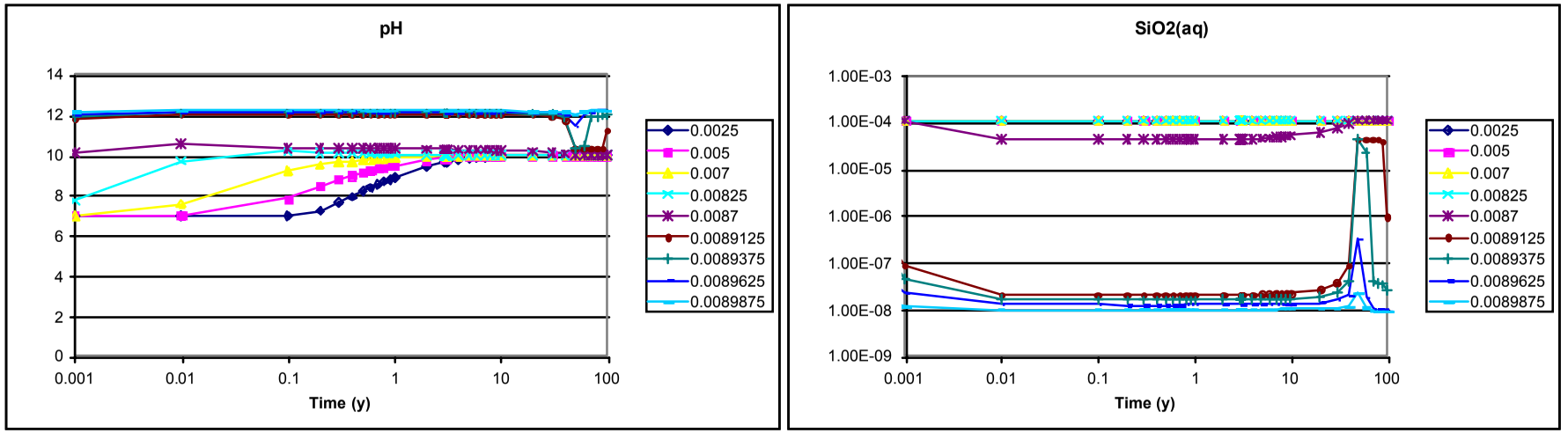

Figure 17 Slow quartz dissolution case: Evolution of pH and SiO_2 in the particle pore water. The colour data points refer to different nodes within the particle, ranging from 0.0025 to 0.0089875 m from the particle centre.

models the region from 100 to 400 μm depth (the 5th cell from the outside) becomes 35 % blocked by 50 years, after which time the amount of blocking remains constant as the region becomes virtually inaccessible to further cement water interaction due to the 100 μm shielding layer. The pore water at this depth is richer in Si and has a lower pH and Ca content, which favours predominantly gyrolite precipitation.

Since there is a far greater precipitation of CSH in this case, the amount of OH^- that is consumed by the particle, and the amount of quartz dissolved in the particle, is approximately an order of magnitude greater than the base case. However the amount of quartz dissolved is still a trivial amount, around 0.05 % of the initial inventory in the particle.

The pore water concentration of Si and the pH is essentially uniform across the first 100 μm depth, the Si concentration being low and the pH being around 12. Si concentration then increases with depth and pH falls to around 10. The sharp peaks in the pore water concentration graphs correspond to the time at which the outer cells become blocked, where pore water concentrations can then rise and fall quickly due to the small amount of pore water in the tiny pore space compared to the large amount of reacting minerals.

In summary, in contrast to what may have been expected, the actual amount of alteration in the interior of the particle is actually greatest in this case where the rate of quartz dissolution is smallest. This is due to the fact that the smaller dissolution rate effectively delays that time taken for the porosity to block. This allows the cement water to penetrate at greater depth into the particle.

The results here demonstrate what might be expected if the quartz dissolution reaction is slower than is anticipated. This could either be due to incomplete understanding of the quartz reaction at high pH, or due to a significantly higher Si content and lower pH in the cement water than is expected. Although the buffering capacity of the particle is increased in this case, the total buffering capacity is still small, as in the base case, so that any significant buffering must take place on the particle surface rather than through diffusion and reaction in the particle pore space.

3.2.3 Summary

In each of the particle-scale models, the total amount of buffering of the cement water provided by diffusion into, and reaction in, the particle pore space is small and is not enough to satisfy the amounts of buffering claimed (for the entire particle, not just the interior) by Karlsson et al (1999). In every case, the interior of the particle becomes shielded from the cement water by a layer of CSH that precipitates in the pore space adjacent to the surface, thus removing the interior of the particle from further reaction.

The implications of these results are that the only area on the particle available for reaction is the externally available surface area. Furthermore, since any small pores in the particle very quickly become filled with CSH, removing the deeper interior of the particle from further reaction, any surface area that is available on a molecular scale should be deemed inaccessible for reaction.

4 Conclusions

Recent work published by SKB on potential reaction mechanisms and assessment of the potential pH buffering capability of gravel backfills (Karlsson et al., 1999) has been reviewed, and scoping calculations to assess likely backfill performance have been carried out.

The approaches and methodologies employed by Karlsson et al. (1999) to model the potential for buffering of hydroxyl ions released by cementitious engineered barriers by reaction with a surrounding gravel barrier are considered to have a number of deficiencies. In particular, their mass balance calculations used a non-conservative estimate of the amount of hydroxyl ions which may be consumed by precipitation of CSH minerals. More conservative choices of the composition of CSH suggest that complete reaction of at least 36 % of the gravel barrier (as currently designed), and possibly much more, would be required to contain the release of all hydroxyl ions contained within cement in SFL 3-5. Also, Karlsson et al.'s scoping calculations overestimate the amount of quartz/SiO_2 likely to be present in the gravel backfill, thus leading to an overestimation of the likely amount of retardation of hydroxyl ion migration through the backfill. Moreover, SKB's calculations assumed that the reactive surface area of particles in the gravel backfill does not change with time and that the rate-limiting step of release of silica remains detachment of silicate ions from the mineral surfaces. However, evidence from SKB's own experiments (Holgersson et al., 1998) suggests that the surface area available for dissolution will decrease with time due to the coating of surfaces by precipitates and it is likely that the rate-limiting step for release of Si (and hence OH^- consumption) ultimately becomes diffusion through an alteration layer of precipitates surrounding rock fragments.

Modelling of quartz-water reactions at the particle-scale using different plausible models for the dissolution of quartz carried out in this study has revealed that the total amount of buffering of the cement water provided by diffusion into, and reaction in, the particle pore space is small and is not enough to satisfy the amounts of buffering claimed by Karlsson et al. (1999). In every model case, the interior of the particle becomes shielded from the cement water by a layer of CSH that precipitates in the pore

space adjacent to the surface, thus removing the interior of the particle from further reaction.

5 References

Bateman, K., Coombs, P., Noy, D. J., Pearce, J., Wetton, P., Haworth, A., and Linklater, C. M., Experimental simulation of the alkaline disturbed zone around a cementitious radioactive waste repository. *In* Chemical Containment of Wastes, (eds. R.M. Metcalfe and C.A. Rochelle), Geological Society Special Publications 157, pp. 183-194, 1999.

Bethke, C.M., *Geochemical Reaction Modelling*. Oxford University Press, 1996.

Brady, P. V., and Walther, J. V., *Controls on silicate dissolution rates in neutral and basic pH solutions at 25 °C* . Geochimica et Cosmochimica Acta 53: 2823-2830, 1989.

Henning, O., and Gerstner, B., *Untersuchungen zur Wechselwirkung zwischen Quarz und Kalziumhydroxid unter hydrothermalen Bedingungen* . W. Zeitschrift der Hochschule Für Architektur und Bauwesen Weimar 19: 53-58, 1972.

Höglund, L. O., and Bengtsson, A., *Some chemical and physical processes related to the long-term performance of the SFR repository*, SKB Progress Report SFR 91-06, Swedish Nuclear Fuel and Waste Management Company, Stockholm, Sweden, 1991.

Holgersson, S., Albinsson, Y., Engkvist, I., Rochelle, C., and Pearce, J., *Interaction of cement pore fluids with host rock and the effect on HTO, Na and Cs diffusion*. Radiochimica Acta 82: 197-203, 1998.

Karlsson, F., Lindgren, M., Skagius, K., Wiborgh, M., and Engkvist, I., *Evolution of geochemical conditions in SFL 3-5*, SKB Report R-99-15 Swedish Nuclear Fuel and Waste Management Company, Stockholm, Sweden, 1999.

Knauss, K. G., and Wolery, T. J., *The dissolution kinetics of quartz as a function of pH and time at 70 °C* . Geochimica et Cosmochimica Acta 52: 43-53, 1988.

Kondo, R., *Kinetic study on hydrothermal reaction between lime and silica*, Autoclaved Calcium Silicate Building Products, Society of the Chemical Industry, 1967.

Rimstidt, J.D., and Barnes, H., *The kinetics of silica-water reactions.* Geochimica et Cosmochimica Acta 44: 1683-1699, 1981.

Savage, D., Bateman, K., Hill, P., Hughes, C., Milodowski, A., Pearce, J., Rae, E., and Rochelle, C., *Rate and mechanism of the reaction of silicates with cement pore fluids*. Applied Clay Science 7: 33-45, 1992.

SKI, Joint SKI and SSI review of SKB preliminary safety assessment of repository for long-lived low- and intermediate-level waste. SKI Technical Report 01:34. Swedish Nuclear Power Inspectorate, Stockholm, Sweden, 2001.

Wolery, T.J., EQ3NR, a computer program for geochemical aqueous speciation-solubility calculations: Theoretical manual, user's guide, and related documentation (version 7.0). Lawrence Livermore Report UCRL-MA-110662 PT III. Lawrence Livermore National Laboratory, Livermore, California, USA, 1992.